Neural Stimulation and Recording Electrodes

Stuart F. Cogan

EIC Laboratories, Inc., Norwood, Massachusetts 02062; email: scogan@eiclabs.com

Annu. Rev. Biomed. Eng. 2008. 10:275–309

First published online as a Review in Advance on April 22, 2008

The *Annual Review of Biomedical Engineering* is online at bioeng.annualreviews.org

This article's doi:
10.1146/annurev.bioeng.10.061807.160518

1523-9829/08/0815-0275$20.00

Key Words

neural prostheses, charge-injection, microelectrodes, electrochemistry, electrode characterization, safe stimulation

Abstract

Electrical stimulation of nerve tissue and recording of neural electrical activity are the basis of emerging prostheses and treatments for spinal cord injury, stroke, sensory deficits, and neurological disorders. An understanding of the electrochemical mechanisms underlying the behavior of neural stimulation and recording electrodes is important for the development of chronically implanted devices, particularly those employing large numbers of microelectrodes. For stimulation, materials that support charge injection by capacitive and faradaic mechanisms are available. These include titanium nitride, platinum, and iridium oxide, each with certain advantages and limitations. The use of charge-balanced waveforms and maximum electrochemical potential excursions as criteria for reversible charge injection with these electrode materials are described and critiqued. Techniques for characterizing electrochemical properties relevant to stimulation and recording are described with examples of differences in the in vitro and in vivo response of electrodes.

Contents

INTRODUCTION

Current and emerging neural prostheses and therapies based on nerve stimulation and recording involve electrodes chronically interfaced to the central and peripheral nervous systems. Applications include upper and lower limb prostheses for spinal cord injury and stroke; bladder prostheses; cochlear and brain-stem auditory prostheses; retinal and cortical visual prostheses; cortical recording for cognitive control of assistive devices; vagus nerve stimulation for epilepsy and depression; and deep brain stimulation (DBS) for essential tremor, Parkinson's disease, epilepsy, dystonia, and depression. All require electrodes characterized by low impedance for recording or safe reversible charge injection for stimulation. The breadth of treatments involving electrical stimulation of neural tissue is reflected in the reviews by Li & Mogul (1), Normann (2), Perlmutter & Mink (3), Clark (4), Shepherd & McCreery (5), Jackson et al. (6), Rutten (7), Jezernik et al. (8), Prochazka et al. (9), Hoffer et al. (10), and Loeb (11). The physiological basis of stimulation has been reviewed by Tehovnik and colleagues (12, 13), McIntyre & Grill (14), and Basser & Roth (15). Applications employing recording electrodes for cognitively controlled prostheses have been reviewed by Lebedev & Nicolelis (16), Friehs et al. (17), and Donoghue (18). Reviews of electrode materials and some aspects of the electrochemistry of stimulation and recording electrodes are found in Merrill et al. (19) and Robblee & Rose (20). A comprehensive review of the literature on the foreign-body response to implanted electrodes and potential adverse consequences is provided in Polikov et al. (21).

DBS: deep brain stimulation

The present article reviews the electrochemical properties required for electrodes used in stimulation and recording of neural tissue with an emphasis on microelectrodes and their electrochemical characterization. Differences in the in vitro and in vivo properties of electrodes are

discussed, and possible methods for the in vivo evaluation of electrodes are described. The review emphasizes those electrode materials that are presently employed in stimulation and recording, and identifies differences in these electrode materials based on their intrinsic electrochemical properties.

Current density (I): the rate of charge injection. For a one-electron faradaic reaction (e.g., $Ir^{4+} + e^- = > Ir^{3+}$)

GSA: geometric surface area

ESA: electrochemical surface area

ELECTRICAL REQUIREMENTS

Stimulation Electrodes

Electrical stimulation initiates a functional response by depolarizing the membranes of excitable cells. Depolarization is achieved by the flow of ionic current between two or more electrodes, at least one of which is in close proximity to the target tissue. In most neural applications, electrical stimulation is applied as a series of biphasic current pulses. Typical pulse waveforms with pulse parameters are shown in **Figure 1**. Each pulse has cathodal and anodal phases, with current amplitudes and durations that result in an overall zero net charge for the pulse (charge-balance). A cathodal current is reducing at the stimulation electrode, with the direction of electron flow being from the electrode to the tissue. Anodal indicates an oxidizing current with electron flow in the opposite direction. The charge delivered is the time integral of the current, which is simply $i_c \cdot t_c$, for a cathodal constant-current pulse of magnitude i_c and pulse width t_c. Charge-balance with intramuscular electrodes and electrodes that interface with the peripheral nervous system is sometimes achieved by a capacitor discharge circuit, leading to a monophasic, capacitor-coupled waveform, which is also shown in **Figure 1**. Current pulses are defined in terms of the charge delivered in the leading phase (q), the charge density in the leading phase (Q_{inj}), the current density (I), the pulse width in each phase, and the pulse frequency. The geometric surface area (GSA) of the electrode is used to define the charge and current densities. The use of electrochemical surface areas (ESAs) has generally not been useful. The ESA can vary greatly depending on the method and conditions used in its measurement, and it is difficult to define for porous electrodes and electrodes with electroactive coatings (22).

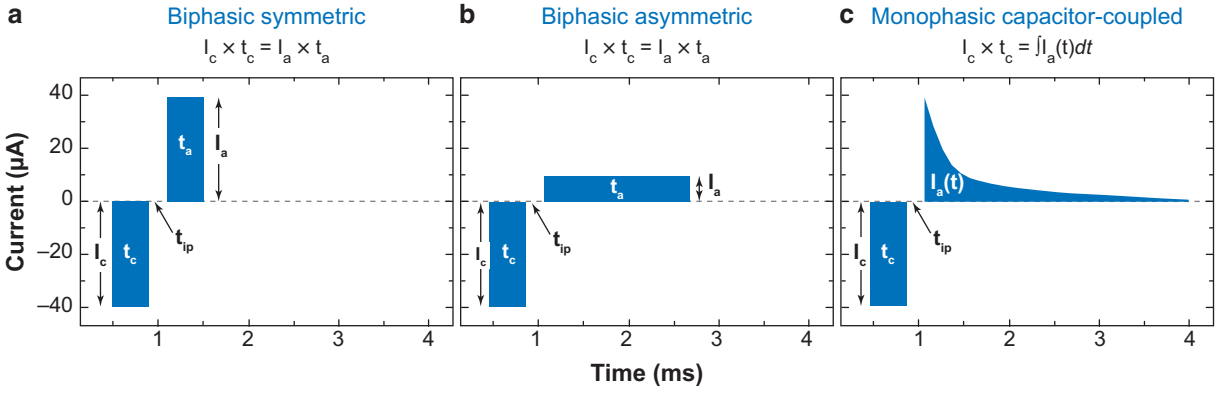

Figure 1

Typical charge-balanced, current waveforms used in neural stimulation. The parameters vary widely depending on the application and size of the electrode. Waveform parameters usually falling in the range of I_c (cathodic current), 1 μA – 10 mA; I_a (anodic current), 1 μA – 10 mA; t_c (cathodic half-phase period), 50 μs – 4 ms; t_{ip} (interphase dwell), 0 – 1 ms; and t_a (anodic half-phase period), 50 μs – 10 ms.

Electrode potential (E): a thermodynamic quantity that measures the driving force for electrochemical reactions at the electrode-electrolyte interface

A number of variations on biphasic current waveforms are possible and have been described (14, 19, 20, 23). For physiological reasons, the leading phase is usually cathodal, although anodal–first pulsing may more efficiently activate populations of some neural elements (24, 25). The use of a slight charge imbalance between the cathodal and anodal charges has also been proposed as a way of compensating for irreversibility in charge-injection processes (26, 27).

The importance of a charge-balanced waveform in avoiding damage to electrodes and surrounding tissue has been recognized for many years (28). Although the approach to achieving charge-balance often emphasized matching the charge in the cathodal and anodal phases of a pulse, it was also recognized that in practice this ideal was not always achieved. The underlying and critical objective of charge-balance is to maintain the electrode potential within a range that does not induce irreversible reduction and oxidation reactions that degrade the electrode, damage tissue, or otherwise limit the charge that can be delivered in a stimulation pulse. However, even if a stimulus pulse pair is charge-balanced, an electrode may be polarized during delivery of the pulse to a point that tissue or electrode-damaging irreversibility occurs. Thus, besides charge balance, stimulus waveforms must be limited to current and charge densities that allow charge injection by reversible processes, which inject cathodic or anodic charge at a finite rate.

The most common irreversible processes encountered with stimulation electrodes are electrolysis of water, with consequent pH changes and gas formation, electrode dissolution due to the oxidative formation of soluble metal complexes [typical of platinum (Pt) electrodes], or the breakdown of passivity and pitting or transpassive corrosion (typical of stainless steel electrodes). Oxidation of organics, such as glucose and tyrosine, or the reduction of oxygen is also possible at potentials encountered with stimulation electrodes under conditions of normal use. Other possible degradation reactions, such as saline oxidation, have been identified, but are not likely unless extremely imbalanced waveforms or large potential excursions are encountered. A comprehensive list of possible irreversible or harmful electrochemical reactions that might occur during stimulation is provided by Merrill et al. (19) and Robblee & Rose (20). For neural stimulation electrodes, in vivo studies have identified Pt dissolution (29, 30) and iridium oxide delamination (31) as electrode degradation processes. Although there is considerable concern regarding tissue damage, the extent of tissue degradation induced by different irreversible processes is not well established.

The clinical usefulness of an electrical stimulation-based neural prosthesis depends on the ability to chronically provide safe levels of therapeutic stimulation. Electrical thresholds for eliciting useful functional responses in animals and humans have been determined for a number of prosthetic applications, and a selection is listed in **Table 1**. The reported thresholds and functionally effective charge densities depend on many factors, and the values in **Table 1** may reflect suboptimal electrode placement or the use of an electrically evoked physiological response as a measure of threshold, rather than a functional response.

In general, electrodes used in neural stimulation can be divided into two categories. Macroelectrodes exhibit high-charge/phase thresholds and low-charge density thresholds; they are typically placed on the surface of the target tissue and have a GSA larger than approximately 100,000 μm^2 (0.001 cm^2). Microelectrodes have the opposite behavior, exhibiting low-charge/phase thresholds and high-charge density thresholds. Microelectrodes typically penetrate the target and have surface areas that are smaller than approximately 10,000 μm^2. An obvious advantage of microelectrodes is the ability to stimulate a comparatively small volume of tissue, which should, with a sufficient number of electrodes, improve the selectivity and spatial resolution of functional responses. Although this classification based on surface area is somewhat arbitrary, most stimulating electrodes fall into one or the other category.

Table 1 Charge/phase and charge density threshold requirements for neural prostheses

Application	Placement	Species	Type	Threshold charge/phase (nC ph^{-1})	Threshold charge density (μC cm^{-2})	Pulse Width (μs)	Reference
Vision	Epi-retinal	Human	Surface	6–1120	5–570	1000	32
Vision	Epi-retinal	Human	Surface	24–100	80–306	2000	33
Vision	Optic nerve	Human	Surface	7–124	4–62	25–400	34
Vision	Intracortical	Human	Penetrating	0.4–4.6	190–2300	200	35
Vision	Cortical	Human	Surface	200,000	11	200	35
Hearing	VCN	Cat	Penetrating	0.75–1.5	60–90	40–150	36, 37
Hearing	AB	Human	Surface[a]	10–200	2.6–52	300	5, 38
Micturition	Intraspinal	Cat	Penetrating	9	4000	100	39
DBS	STN	Human	Penetrating[b]	135–400	2.3–6.7	60–200	40
Motor	Intrafascicular	Cat	Penetrating	4[c]	0.5	50	41
Motor	Sciatic nerve	Cat	Penetrating	5[c]	96	200	42
Motor	Sciatic nerve	Cat	Surface	46	0.35	200	42

[a]Auditory brain stem prostheses are essentially surface electrodes, deeply implanted but placed on the surface of the target neural structure.
[b]Although DBS electrodes penetrate the brain, in current clinical devices the electrodes have large areas (0.06 cm^2) and behave as macroelectrodes.
[c]The electrodes were implanted within the tibial nerve, but are large (GSA = 0.008 cm^2). The result in a relatively low charge/phase threshold because of the close proximity of the electrode and neural elements within the fascicles and a low charge density threshold because of the large area.
VCN, ventral cochlear nucleus; AB, auditory brainstem; STN, subthalamic nucleus.

Macroelectrodes, with their modest charge-injection densities, do not typically corrode or exhibit stimulation-induced electrode degradation when subjected to clinically relevant levels of charge. The high-charge/phase levels, however, may induce tissue damage, which is generally more of a concern than corrosion with surface electrodes. For microelectrodes, charge densities are high and electrode degradation as well as tissue damage are encountered. The charge/phase and charge density each contribute to stimulation-induced tissue damage and both must be known to predict whether stimulation might be harmful to tissue (43). An extensive study of safe and effective stimulation levels for surface and penetrating brain electrodes has been conducted at the Huntington Medical Research Institutes. These studies suggest a narrow safe window for penetrating microelectrodes (GSA $\leq$ 2000 μm^2) in the brain with charge/phase thresholds of $\sim$1 nC ph^{-1} for eliciting neuronal excitation in the feline cochlear nucleus and cerebral cortex (37, 44, 45), whereas histologically observed tissue damage is absent at 2 nC ph^{-1} but present at 4 nC ph^{-1} (800 μC cm^{-2}). Kuncel & Grill (40) reviewed functional and tissue damage thresholds for the macroelectrodes used in clinical DBS (GSA = 0.06 cm^2). The estimated charge density at these electrodes is $<$10 μC cm^{-2} ($\sim$0.5 μC ph^{-1}) at clinically effective levels, which is well below reported tissue damage thresholds for large-area electrodes. However, as pointed out by Kuncel & Grill (40), most tissue damage thresholds have been determined at frequencies well below those employed in DBS, and caution should be exercised in extrapolating between different stimulation protocols.

Recording Electrodes

The activity of neurons is recorded as an extracellular potential, or action potential, when the recorded signal identifies the firing of a single neuron (single-unit). Action potentials are recorded

PEDOT: poly(ethylenedioxythiophene)

with microelectrodes implanted in close proximity to the target neurons, and, for single-unit recording, the microelectrode GSA should be no larger than approximately 2000–4000 μm^2, and is typically much smaller. Such neural recordings, particularly from large ensembles of neurons, are the basis of prostheses that could provide cognitive control of external prosthetic devices to aid patients with paralysis (16, 18, 46). Other applications for multielectrode neural recordings, in which the recorded neural signals determine the output of implanted stimulation electrodes, are also contemplated and include adaptive DBS (47) and functional stimulation for epilepsy (48).

The objective with single-unit neural recording is to measure action potentials with a useful signal-to-noise ratio, ~5:1 or greater, and to do this chronically. The amplitude of action potentials in the CNS can be quite large, more than 500 μV, but is more typically on the order of 100 μV, and often is smaller (49–52). In general, the majority of the noise signal encountered in single-unit recording arises from the multitude of undifferentiated background action potentials (neural noise). However, electrode impedance does contribute noise, and higher impedance electrodes are expected to have a lower signal-to-noise ratio. In addition, high electrode impedance in combination with the distributed capacitance between the electrode and the recording amplifier will reduce the electrodes' high-frequency response (53).

A wide range of materials has been used for recording electrodes, including stainless steel, tungsten, platinum, platinum-iridium alloys, iridium oxide, titanium nitride, and poly(ethylenedioxythiophene) (PEDOT). Recording electrodes are typically characterized by their impedance at 1 kHz, which is quite variable, ranging in vivo from approximately 50 kΩ to 1 MΩ. Although current flow across the electrode-electrolyte interface is minimal for recording electrodes, and so there are no high-rate electrochemical challenges to the electrode, maintaining consistent neural recordings with chronically implanted microelectrodes has been difficult (21, 54). The distance between a neuron and electrode, and the respective sizes of each, will always affect the quality of a neural recording. However, many other factors that include the impedance of the electrode and the thickness and composition of the connective tissue sheath surrounding the electrode are important and may vary with time following implantation. Fabrication and design difficulties with multielectrode arrays have contributed to the inconsistent performance, but the tissue response to the implanted electrode is probably the primary cause. The adverse tissue response can arise from insertion trauma (55), an intrinsic foreign-body response to the electrode material (56–58), or micromotion of the electrode (59, 60).

Although in vitro studies have clearly shown that biomolecular and cellular interactions increase the impedance of recording microelectrodes (61), in vivo studies suggest a less certain correlation between electrode impedance (at 1 kHz) and recording quality (52). Instructively, in the study by Suner et al. (52), single-unit recordings were obtained for up to 1.5 years in monkey motor cortex, with an average of 85 of 96 electrodes in one animal providing fair to good recordings, although the subset of electrodes providing the recordings varied over the course of the study. The lack of consistent performance of the single-unit recordings, which may have little to do with the properties of the electrodes themselves, has led to the adoption of cortical ensemble or multiunit recording methods to provide more stable control signals for prosthetic devices (62, 63).

A more biologically based approach to establishing a recording interface with neurons has been described by Kennedy and colleagues (64, 65). A section of sciatic nerve or neurotrophic factor is incorporated into a hollow glass cone containing a metal wire electrode. The neuro-attractive elements promote ingrowth of neurites into the cone, and these electrodes have been used for neural recording in both chronic animal and human studies (66). Although the cone electrodes are not recent in their development, they presage a variety of tissue engineering approaches to promoting chronically stable nerve-electrode interfaces (67–69).

CHARGE-INJECTION MECHANISMS AND ELECTRODES FOR STIMULATION

Faradaic reaction: an electrochemical reaction in which chemical species are oxidized or reduced

Charge-injection capacity (Q_{inj}): the amount of charge per unit GSA delivered in the leading phase of a stimulation pulse

Electrodes are metallic conductors and reactions at the electrode-tissue interface are required to mediate the transition from electron flow in the electrode to ion flow in the tissue. These reactions can be capacitive, involving the charging and discharging of the electrode-electrolyte double layer, or faradaic, in which surface-confined species are oxidized and reduced. Capacitive charging can be either electrostatic, involving purely double-layer ion-electron charge separation and electrolyte dipole orientation, or electrolytic, involving charge stored across a thin, high-dielectric-constant oxide at the electrode-electrolyte interface. Faradaic reactions involve the transfer of an electron across the electrode-electrolyte interface and require that some species, on the surface of the electrode or in solution, undergo a change in valence, i.e., are oxidized or reduced. For noble metal electrodes, primarily Pt and PtIr alloys, the faradaic reactions are confined to a surface monolayer, and these reactions are often described as pseudocapacitive, although electron transfer across the interface still occurs (70). Charge can also be stored and injected into tissue from valence changes in multivalent electrode coatings that undergo reversible reduction-oxidation (redox) reactions. These coatings, which are typified by iridium oxide, but include newer materials such as poly(ethylenedioxythiophene), are mixed conductors, exhibiting both electron and ion transport within the bulk of the coating. The three-dimensional structure of the coatings provides more charge for stimulation, but access to this charge is limited by the rate of electron and ion transport within the coating.

The nature of the reactions that provide charge injection is shown schematically in **Figure 2** for the most commonly employed capacitive, monolayer faradaic (pseudocapacitive), and coating-based faradaic charge-injection electrodes. Each charge-injection mechanism is described in more detail in the following sections using those electrode materials that are currently being used for neural stimulation as illustrative examples. Some relevant properties of electrode materials are collected in **Table 2**.

Capacitive Charge-Injection Materials

In principle, capactive charge-injection is more desirable than fardaic charge-injection because no chemical species are created or consumed during a stimulation pulse. Because the double-layer charge per unit area at an electrode-electrolyte interface is small, high charge-injection capacity is only possible with capacitor electrodes that are porous or employ high dielectric constant coatings. Both strategies have limitations.

Titanium nitride. Titanium nitride (TiN) is a chemically stable metallic conductor with good biocompatibility. Charge is injected through the electrode-electrolyte double layer, and large charge-injection capacities (Q_{inj}) are obtained by fabricating electrodes with a high surface roughness such that the ESA greatly exceeds the GSA. In many respects, porous TiN exhibits the ideal features elucidated by Guyton & Hambrecht (80) and Rose et al. (76) for intracortical capacitor electrodes, with the difficulty of obtaining high ESAs in microelectrodes of small GSA being overcome by the use of sputter deposition to produce a highly porous (sometimes called fractal) geometry. An example of the porous morphology of a high surface area sputtered TiN electrode is shown in **Figure 3**. Weiland et al. (78) have reported an in vitro charge-injection capacity of 0.9 mC cm^{-2} (0.5-ms pulse width) for 4000 μm^2 TiN electrodes. This is less than the charge injection capacity of some faradaic electrode coatings, such as iridium oxide, but higher charge capacities may be possible with TiN electrodes having a higher ESA/GSA ratio. The potential

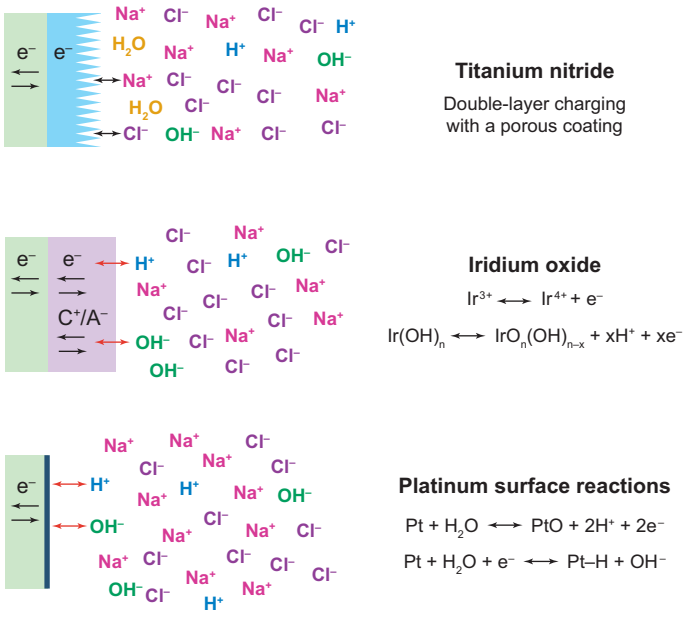

Figure 2

Capacitive (TiN), three-dimensional faradaic (iridium oxide), and pseudocapacitive (Pt) charge-injection mechanisms.

Table 2 Charge-injection limits of electrode materials for stimulation in the CNS

Material	Mechanism	Maximum Q_{inj} (mC cm^{-2})	Potential Limits V versus Ag|AgCl	Comments	References
Pt and PtIr alloys	Faradaic/capacitive	0.05–0.15	−0.6–0.8		71
Activated iridium oxide	Faradaic	1–5	−0.6–0.8	Positive bias required for high Q_{inj}. Damaged by extreme negative potentials (<−0.6 V)	72, 73
Thermal iridium oxide	Faradaic	~1	−0.6–0.8 V	Positive bias required for high Q_{inj}	74
Sputtered iridium oxide	Faradaic	1–5	−0.6–0.8 V	Benefits from positive bias. Damaged by extreme negative potentials (<−0.6 V)	75; S.F. Cogan, J. Ehrlich, T.D. Plante, A. Smirnov, D.B. Shire, M. Gingerich, J.F. Rizzo, unpublished
Tantalum/Ta_2O_5	Capacitive	~0.5		Requires large positive bias	76, 77
Titanium nitride	Capacitive	~1	−0.9 to 0.9	Oxidized at positive potentials	78
PEDOT	Faradaic	15	−0.9 to 0.6	Benefits from positive bias	79

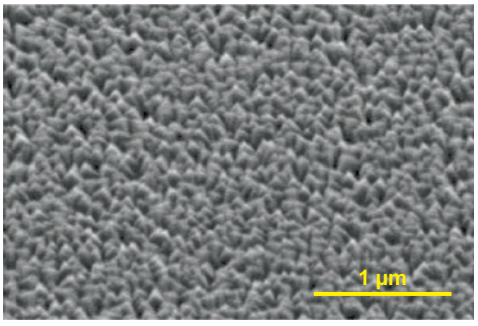

Figure 3

Scanning electron micrograph of the porous surface of sputtered TiN that gives rise to a high ESA/GSA ratio.

limits for avoiding irreversible reactions on TiN are wider than those for Pt or Ir oxide, with water reduction and oxidation potentials of −0.9 V and 0.9 V (versus Ag|AgCl), respectively, as measured by slow-sweep-rate cyclic voltammetry (CV). Fractal TiN, with a very high ESA, is used extensively as a coating for cardiac pacing electrodes, primarily because the electrode polarization during a pacing pulse is minimal, allowing the electrode to sense the cardiac contraction in the interpulse period (81, 82).

Porous TiN electrodes, and equivalently any electrode with a high ESA/GSA ratio, have a large charge storage capacity (CSC) as measured at low rates by slow-sweep-rate CV. However, under the high rate, high current density conditions of a neural stimulation pulse, access to all the available charge is limited by pore resistance (82–84). For all high–surface area electrodes, pore resistance imposes a geometric limitation on the increase in charge-injection capacity that can be obtained by increasing the ESA/GSA ratio. A schematic view of a pore and electrolyte in a porous electrode coating is shown in **Figure 4**. The electrolyte resistance and capacitance on the interior surface of the pore combine to form a delay-line with a time-constant defined by the pore geometry, electrolyte resistivity, and the interfacial double-layer capacitance. The consequence of this time-constant is that the total ESA of the electrode is not accessed at the current densities encountered during stimulation. Narrower and deeper pores give rise to higher time-constants, and their charge-injection capacity is more difficult to access than that of electrodes with shallow pores.

A useful feature of TiN is the intrinsic chemical and mechanical stability of the coating. TiN is not sensitive to dehydration, can be sterilized by common methods, and is easily stored and shipped, wet or dry. Porous TiN also may be patterned photolithographically and is suitable for flexible substrates, making it a candidate for intracortical silicon microprobes, retinal electrode arrays, and some nerve cuffs designs.

CV: cyclic voltammetry

Charge storage capacity (CSC): the total amount of charge per unit GSA available from an electrode. Cathodal (CSC_c) and anodal (CSC_a) values can be defined

Tantalum/tantalum oxide. The charge-injection capabilities of a capacitor electrode can be increased beyond that available from the charge in the electrode-electrolyte double layer by the use of a dielectric coating. Tantalum/tantalum oxide capacitor electrodes have been the most extensively studied for nerve electrodes, and their use has been reviewed by Rose et al. (76). To achieve useful levels of charge-injection, a large ESA/GSA ratio is still required, and the high-rate charge-injection capacity is limited by pore resistance. Valve metal capacitor electrodes, primarily Ta/Ta_2O_5 and Ti/TiO_2, although the subject of extensive earlier investigations, are not used extensively. There are several disadvantages of Ta/Ta_2O_5 electrodes, including difficulty

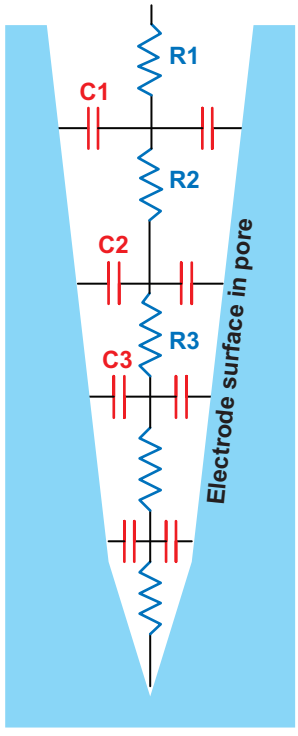

Figure 4

Schematic view of a pore cross-section showing the pore resistance (R1..R3) and double-layer capacitance (C1..C3) elements that give rise to a delay-line and time-constant for accessing all the ESA and its associated double-layer capacity.

in achieving adequate ESA/GSA ratios, limited charge-injection due to pore resistance, and the need for relatively high bias voltages (>4 V) in the interpulse period (77). However, Ta/Ta_2O_5 has been used successfully as a combination electrode and charge-storage element in the Bion™ implantable stimulator (85, 86).

Faradaic Charge-Injection Materials

The reduction and oxidation reactions at faradaic electrodes provide high levels of charge for stimulation. However, changes in the electrolyte composition adjacent to the electrode and the finite rate of faradaic reactions can lead to irreversible processes that cause electrode or tissue damage. The selection of charge injection waveforms for stimulation must be carefully considered to avoid these damaging reactions.

Noble metals. The noble metals of choice for neural stimulation are Pt and PtIr alloys. These metals inject charge by both faradaic reactions and double-layer charging. The relative contribution of each process depends on the current density and pulse width, although the faradaic processes predominate under most neural stimulation conditions. In early work, Brummer & Turner (28) determined Pt charge-injection limits of 300–350 μC cm^{-2} based on double-layer charging, the reversible faradaic processes of hydrogen atom deposition and oxidation, and surface oxidation

and reduction. However, these limits were determined at lower current densities (<0.45 A cm^{-2}) and longer pulse widths (>0.6 ms) than are generally employed in neural stimulation. Using 0.2-ms pulses, Rose & Robblee (71) determined limits of 50–150 μC cm^{-2} to avoid reduction or oxidation of water that occur at approximately −0.6 V and 0.8 V (Ag|AgCl), respectively, at pH 7. Cogan et al. (87), in an in vitro study of PtIr-alloy microelectrodes, found a bias-dependent, cathodal charge-injection limit, based on avoiding water electrolysis, that increased from 90 μC cm^{-2} to 300 μC cm^{-2} as the bias was increased from 0.1 V to 0.7 V (Ag|AgCl). Although the use of a positive interpulse bias to increase cathodal charge-injection limits is well established for activated iridium oxide films (AIROFs) (72, 73), the long-term stability of PtIr or Pt at bias levels that are positive of the equilibrium potential of the metal is unknown. Donaldson & Donaldson (88, 89) provided an interesting historical background to the development of Pt electrodes with a pragmatic view of charge-balanced waveforms, reflecting earlier comments that limiting the electrode potential to within safe limits is a more important objective than achieving a well-balanced waveform. It may also be easier electronically to design pulse generators to avoid electrode potential excursions beyond the water window than to ensure that the stimulus is precisely charge-balanced.

AIROF: activated iridium oxide film

In vivo, a Pt electrode establishes a rest potential of approximately 0 V versus Ag|AgCl (90), and the total charge available for cathodal stimulation is reduced to that between 0 V and −0.6 V (Ag|AgCl). Thus Pt or PtIr alloy electrodes, which have a theoretical charge-injection capacity of 300–350 μC cm^{-2}, can only inject ∼100 μC cm^{-2} without exceeding the water reduction potential (71, 87). Although the charge-injection limits of Pt are based on avoiding electrolysis of water, Pt dissolution can occur at lower charge densities. For example, Pt dissolution was observed in vivo at charge densities of 20–50 μC cm^{-2} and dissolution rates of 38 ng h^{-1} were measured with 0.1 cm^2 smooth Pt electrodes pulsed at 100 μC cm^{-2} (30). Adsorbed protein markedly reduces Pt dissolution, so lower dissolution rates are expected in vivo compared with in vitro pulsing at equivalent charge levels (91, 92).

The cochlear implant, perhaps the most successful neural prosthesis, employs Pt as a stimulation electrode; the electrodes are large, and typical charge densities do not exceed 20 μC cm^{-2} (90 nC ph^{-1}, GSA ∼ 0.4 mm^2) when using biphasic, charge-balanced current pulses. With a view to providing a large number of small-area charge-injection sites on cochlear electrode arrays, Tykocinski et al. (93) investigated high ESA/GSA ratio (HiQ) Pt electrodes. The HiQ electrodes were effective in reducing electrode polarization during stimulation and also reduced the magnitude of the current flowing between pulsed electrode pairs that were shorted during the interpulse period. More recent efforts to employ moderately porous films of Pt that can inject charge at >1 mC cm^{-2} have also been reported (94). These "Pt gray" films have the advantage of improved abrasion resistance relative to the more familiar Pt black, which is rarely used for neural stimulation.

Iridium oxide. Noble metal alloys may be used for intracortical or intraspinal stimulation, but their charge-injection capacities are marginal for applications requiring stimulation with microelectrodes. The need for microelectrodes with higher charge-injection capacities led to the development of faradaic electrode coatings based on films of hydrated Ir oxide (95). The first Ir oxide coatings were formed by electrochemical activation of Ir metal to form AIROFs (see AIROF Activation sidebar). By repeated oxidation and reduction of Ir, a hydrated oxide film can be formed on the metal surface that greatly increases its ability to inject charge by a fast and reversible faradaic reaction involving reduction and oxidation between the Ir^{3+} and Ir^{4+} states of the oxide (96). The ability of Ir oxide to inject charge efficiently during pulsing at high charge density can also be increased by applying a positive bias of 0.4–0.8 V (versus Ag|AgCl) in the interpulse period (72). The bias polarizes the Ir oxide from a mixed Ir^{3+}/Ir^{4+} valence state to the Ir^{4+} valence state, which

AIROF ACTIVATION

A typical Ir activation protocol involves rectangular potential pulsing between limits of −0.6 V and 0.85 V versus Ag|AgCl in phosphate buffered saline (PBS) at pH 7.4. The pulse frequency can range from 1 Hz to 0.05 Hz, corresponding to a half-phase pulsewidth of 0.5 s and 10 s, respectively, at each potential limit. The rate at which the cathodal charge storage capacity (CSC_c) increases with pulsing varies with the GSA of the electrode, the pulse frequency, and the potential limits. The CSC_c increases approximately linearly with the number of pulses, with rates of 0.02–0.05 mC cm^{-2}-pulse being typical. For example, a 2000 μm^2 Ir electrode activated in PBS between limits of −0.6 and 0.85 V at 0.25 Hz reaches a CSC_c of 25 mC/cm^2 after 900 pulses. Large electrodes activate more slowly than small electrodes and low frequency pulsing promotes more uniform activation. The use of a well-buffered electrolyte, such as PBS, is necessary to obtain useful activation rates and, consequently, in vivo activation of iridium is difficult. AIROF electrodes fabricated from polymer-insulated iridium wire, similar to that shown in **Figure 5**, are used extensively for stimulation studies in cerebral cortex and spinal cord (39, 45, 97). AIROF electrodes are also used on silicon microprobes fabricated by thin-film silicon micromachining technology (98). With Si microprobes, the AIROF is formed by activation of sputtered Ir metal films with no apparent difference in properties between AIROF formed from wire or thin-film coatings. AIROF coatings have been used clinically for acute and short-term chronic (four month) studies of intracortical stimulation of the visual cortex (35, 99). There was significant attrition of electrodes in the chronic study due to breakage of lead wires, but intact electrodes could generate phosphenes over a four-month period.

is substantially more electronically conducting and makes available more Ir^{4+} for reduction during cathodal pulsing. At least a factor of three increase in charge capacity can be realized with anodic biasing (73).

SIROF: sputtered iridium oxide film

Ir oxide films can also be formed by reactive sputtering from Ir metal in an oxidizing plasma. Sputtered iridium oxide films (SIROFs) have been investigated for neural stimulation electrodes by Klein et al. (100) who assessed the relationship between sputtering conditions, charge capacity, and surface morphology of SIROFs. In these early studies, no charge-injection limits for current pulsing were reported, although extensive control of film morphology was demonstrated. More

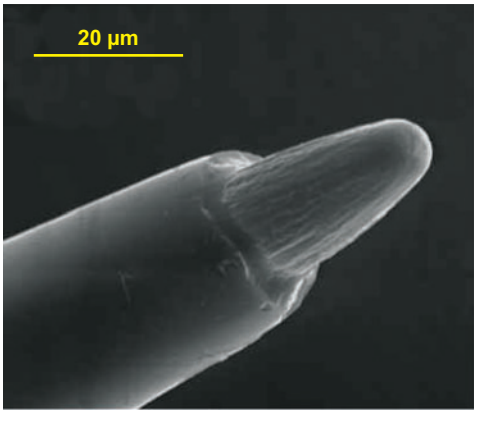

Figure 5

An AIROF microelectrode for intracortical stimulation and recording.

recently, charge-injection capacities of 100 $\mu C\ cm^{-2}$ and higher were reported by Slavcheva et al. (101) for 200-nm-thick SIROFs using relatively long 10-ms pulses. Cogan et al. (75) reported charge-injection limits of 750 $\mu C\ cm^{-2}$ using 0.75-ms pulses with DC-sputtered SIROF on 0.05-cm^2 electrodes. Wessling et al. (102) evaluated the effects of deposition conditions on the morphology of RF-sputtered SIROF intended for neural stimulation applications. S. Cogan, J. Ehrlich, T. Plante, A. Smirnov, D. Shire, et al. (unpublished data) have measured the charge-injection capacity of SIROF as a function of electrode area and thickness. The SIROF charge-injection capacities were comparable with AIROF, approximately 5 $mC\ cm^{-2}$ with 2000-μm^2 electrodes (100 $nC\ ph^{-1}$) using 400-μs pulses and a 0.6 V versus Ag|AgCl interpulse bias. The maximum SIROF charge-injection capacity (Q_{inj}) exhibits a similar bias dependence as AIROF but, advantageously, maintains a notably higher charge-injection capacity at more negative potentials (<0.4 V versus Ag|AgCl).

Emerging Materials

Recently, intrinsically conducting polymers and carbon nanotubes have emerged as alternatives to Pt, Pt alloys, Ir oxide, and TiN as materials for chronic stimulation and recording. An important aspect of these new materials is the possibility of chemical surface modification with physiologically active species to enhance the biocompatibility and the functionality of the electrodes.

Poly(ethylenedioxythiophene). PEDOT is an electrically conducting polymer (ECP) that, like iridium oxide, exhibits both electronic and ionic conductivity. Early work on ECPs for neural stimulation focused on polypyrrole and was not promising. For example, films of polypyrrole electropolymerized on Pt exhibited poor rate capability, requiring a 5-ms pulse to inject 250 $\mu C\ cm^{-2}$ during controlled current pulsing, and delaminated from the Pt at higher charge densities. An improvement in charge-injection capacity and stability was obtained with anthraquinone modifications to the polypyrrole, but pulse widths of 10 ms were still required to inject reasonable charge levels (1.3 $mC\ cm^{-2}$) (103). The emergence of Ir oxide and TiN, with their clearly superior charge injection capabilities, ended interest at that time in ECPs for neural stimulation.

There has been a recent resurgence in the study of ECPs for nerve electrodes with emphasis on their modification with biomolecules to enhance biocompatibility and provide a biologically active interface between the electrode and tissue (104, 105). PEDOT has emerged as the most promising of the ECPs (106). Anion doping of PEDOT (i.e., $PEDOT^+A^-$ formation) is necessary to obtain the high electronic conductivity required for low-impedance recording or for charge-injection, with most studies employing poly(styrene sulfonate) (PSS) as the dopant, which is incorporated into the polymer during the electropolymerization process. The PSS is physically entrained in the PEDOT and forms a charge-transfer complex that results in oxidation of the PEDOT and consequent high electronic conductivity. A significant reduction in electrode impedance is obtained with PEDOT-PSS coatings, and neural recordings from PEDOT-coated microelectrodes have been demonstrated in chronic studies (107). Extensive control of the morphology, incorporation of biomolecules, and the possibility of in vivo polymerization of PEDOT have been demonstrated (108–110).

The charge-injection capabilities of PEDOT for neural stimulation have only been briefly reported. Nyberg et al. (111) demonstrated a charge-injection capability of 3.6 $mC\ cm^{-2}$ with PEDOT-PSS coatings on tin-doped indium oxide (ITO) electrodes (GSA = 2500 μm^2) with 1 ms, 0.5 V pulses. In recent studies, the charge-injection capacity for PEDOT-PSS on PtIr or Au microelectrodes (GSA ~ 2000 μm^2) was found to be approximately 15 $mC\ cm^{-2}$ (0.4-ms cathodal pulses), approximately three times that available with AIROF or SIROF electrodes of similar

geometry (79). This result suggests that PEDOT coatings could be useful for microelectrodes with particularly small GSAs, <500 μm^2, that would be suitable for both stimulation and single-unit recording from small neurons. Whether PEDOT injects charge by capacitive or faradaic processes depends on the potential range over which the electrode is driven during pulsing. For potentials more positive than −0.6 V Ag|AgCl, capacitive charge-injection may dominate, although the details of the charge-injection processes in PEDOT at high current densities have not been fully explored.

PBS: phosphate buffered saline, used extensively for in vitro testing. In the present work, PBS is 126 mM NaCl, 22 mM NaH_2PO_4-$7H_2O$, and 81 mM Na_2HPO_4-H_2O at pH 7.3 and is purged with argon to remove oxygen

Carbon nanotubes. Carbon nanotubes are attractive as neural electrodes because of the high ESA/GSA ratio inherent in the nanotube geometry, which gives rise to a large double-layer charge capacity. For neural stimulation, Wang et al. (112) have found charge-injection capacities of 1–1.6 mC cm^{-2} with vertically aligned nanotube electrodes, and work on the development of nanotube and nanofiber neural interfaces has been reported (113). Carbon nanotubes may also be chemically modified to enhance biocompatibility or provide other functional properties (114).

ELECTRODE CHARACTERIZATION

The common techniques for electrochemical characterization of nerve electrodes are CV, impedance spectroscopy, and potential transient measurements. These techniques can be applied in vitro or in vivo and are described below with illustrative examples.

Cyclic Voltammetry

CV is a three-electrode measurement in which the potential of a test electrode, with respect to a noncurrent-carrying reference electrode, is swept cyclically at a constant rate between two potential limits while allowing current to flow between the test electrode and a counterelectrode. The potential provides the driving force for reactions at the test electrode, while the current is proportional to the rate of these reactions. CV identifies the presence of electrochemical reactions and provides information on the reversibility of the reactions, the quantity of electroactive material on the electrode, and the stability of the electrode. It is important to appreciate that the CV response, for any electrode material, can appear very different depending on the sweep rate, the geometric area of the electrode, and the roughness of the electrode, even though the electrochemical reactions are unchanged.

It has become common practice to characterize stimulation electrodes by their cathodal CSC (CSC_c). The CSC_c is calculated from the time integral of the cathodic current in a slow-sweep-rate cyclic voltammogram over a potential range that is just within the water electrolysis window. For Pt and Ir oxide electrodes, the water window is typically taken as −0.6 V to 0.8 V versus Ag|AgCl. The shaded region in the AIROF CV in **Figure 6** represents a CSC_c of 23 mC cm^{-2}, calculated at a sweep rate of 50 mV s^{-1}, noting that the potential axis is related to time through the sweep rate.

Cyclic voltammograms obtained in phosphate buffered saline (PBS) from identically sized macroelectrodes of Pt, SIROF, and a smooth sputtered TiN film are compared in **Figure 7**. The TiN voltammogram has the approximately rectangular shape that is expected for an electrode exhibiting only double-layer capacitance. The Pt CV exhibits distinct peaks associated with the oxidation and reduction of a surface oxide (peaks 1 and 2, respectively) and hydrogen-atom plating and stripping (peaks 3 and 4, respectively). Double-layer charging also contributes to the capacity of the Pt and is apparent around −0.2 V in **Figure 7**, where there are no obscuring faradaic processes. The significantly higher charge storage capacity obtained with three-dimensional

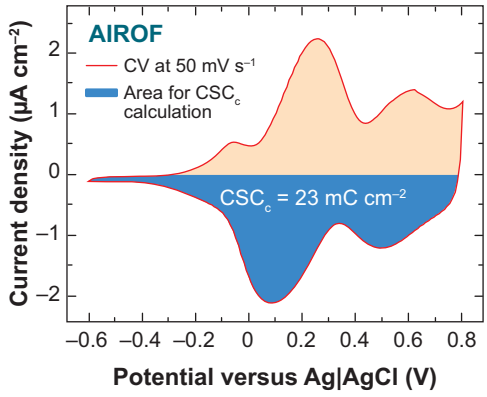

Figure 6

A CV of AIROF in phosphate buffered saline (PBS) at 50 mV s^{-1}. The time integral of the negative current, shown by the blue region of the voltammogram, represents a CSC_c of 23 mC cm^{-2}.

electrode coatings is reflected in the CV of the SIROF electrode. Although the SIROF is only ~10 nm thick, it has more than five times the available charge for the same GSA. The SIROF CV has a rectangular shape suggestive of capacitive behavior, but the charge is substantially faradaic involving the reversible Ir^{3+}/Ir^{4+} couple (115). The CSC_c of the electrodes in **Figure 7** are 250 μC cm^{-2}, 550 μC cm^{-2}, and 2.8 mC cm^{-2} for TiN, Pt, and SIROF, respectively.

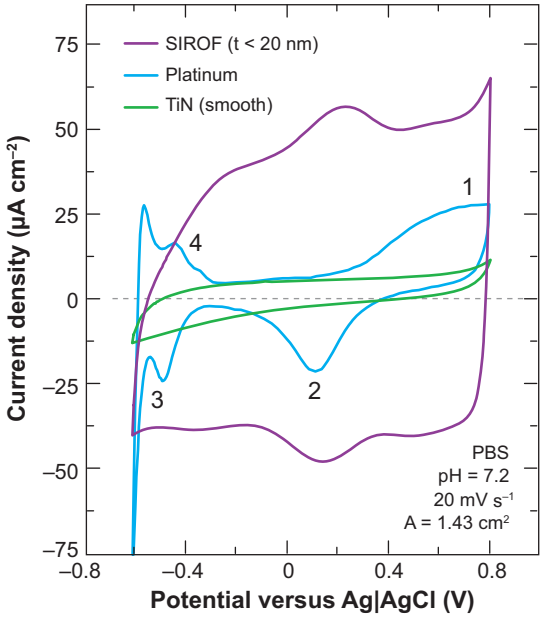

Figure 7

Comparison of cyclic voltammograms of platinum, SIROF, and smooth TiN macroelectrodes (GSA = 1.4 cm^2) in PBS at a sweep rate of 20 mV s^{-1}. 1, 2 indicate Pt oxidation and reduction; 3, 4 indicate hydrogen atom plating and stripping on Pt, respectively. The cathodic charge storage capacities (CSC_c) of the films are 0.25 mC cm^{-2}, 0.55 mC cm^{-2}, and 2.8 mC cm^{-2} for TiN, Pt, and SIROF, respectively.

The CSC_c is essentially a measure of the total amount of charge available for a stimulation pulse. However, the CSC_c, which is obtained under low-current-density, near-equilibrium conditions, has limitations as a predictor of charge-injection capacity for neural stimulation. As described previously for Pt, an implanted electrode establishes an equilibrium potential that is intermediate between the upper and lower potential limits used to generate the cyclic voltammograms for the CSC_c integration. AIROF, for example, has an in vivo equilibrium potential close to 0.0 V (Ag|AgCl), and without the use of a positive bias provides only a modest advantage over Pt for stimulation (87). Other factors, such as pore resistance and activation overpotential, which are most relevant at high current densities, also reduce the charge-injection capacity of an electrode relative to the CSC_c. With typical stimulation parameters, between 5%–20% of the equilibrium CSC_c of AIROF can be delivered in a cathodal current pulse without exceeding the water reduction potential.

An instructive example of how the dependence of CSC_c on sweep rate may be used in vivo to assess the condition of an electrode is shown in **Figure 8**. In this example, a single-shaft, Parylene-insulated AIROF microelectrode is implanted in cat cortex. The electrode has a GSA of ~2000 μm^2 (see **Figure 5**). CVs were acquired at 50 mV s^{-1} and 50,000 mV s^{-1} within one day following implantation and after six weeks using an implanted Ag|AgCl reference and Pt counterelectrode. At the 50 mV s^{-1} sweep rate, at currents of <40 nA, there is a pronounced increase in the apparent CSC_c of the microelectrode after six weeks. However, for the same

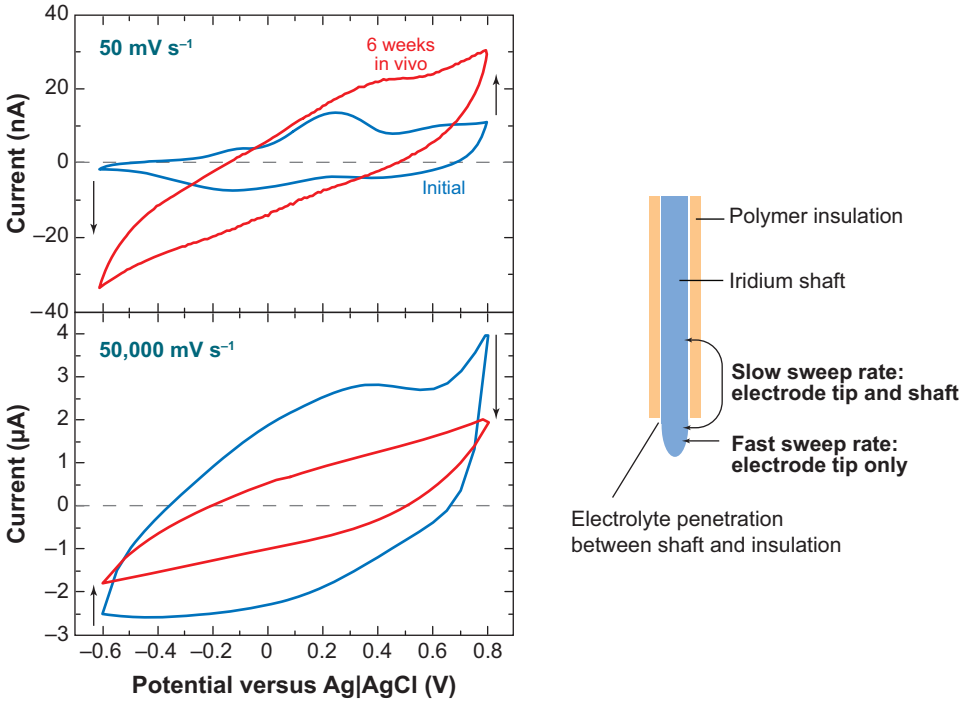

Figure 8

A comparison of the difference in response of 50 mV s^{-1} and 50,000 mV s^{-1} CVs of an AIROF microelectrode implanted in cat cortex within one day following implantation and six weeks after implantation. The 50 mV s^{-1} CV increases in capacity due to electrolyte leakage under the Parylene insulation, whereas tissue encapsulation reduces the CV capacity at 50,000 mV s^{-1}.

electrode at 50,000 mV s^{-1} there is pronounced decrease in CV charge capacity over six weeks of implantation. The explanation for this observation is provided schematically in **Figure 8**. Over the six-week period, electrolyte penetrates under the Parylene insulation, increasing the effective area of the electrode and correspondingly increasing the 50 mV s^{-1} CSC_c. At the high sweep rate, however, pore resistance limits the accessibility of the electrode area under the insulation and the CV provides information only on the exposed electrode tip. In this example, which was typical of a large number of electrodes in this study, biomolecule absorption or tissue encapsulation resulted in a decrease in the 50,000 mV s^{-1} CSC_c. Thus, CVs at high sweep rates provide information primarily on exposed areas of the electrode, whereas CVs at slow sweep rates include contributions from more occluded areas of the electrode. For AIROF electrodes, a very distinctive change in the shape of the CV (50 mV s^{-1}) also occurs when the electrode is overpulsed to potentials more negative than −0.6 V (Ag|AgCl). The shape change is observed in vitro and in vivo and has been attributed to delamination or microcracking of the AIROF (31, 116).

Impedance Spectroscopy

Electrochemical impedance spectroscopy (EIS) involves measuring the electrical impedance and phase angle obtained with sinusoidal voltage or current excitation of the electrode. The measurement is made over a broad frequency range, typically <1 Hz to 10^5 Hz, and the magnitude of the excitation is sufficiently small that a linear current-voltage response is obtained at each frequency. For voltage excitation, the root-mean-square magnitude of the excitation source is typically ∼10 mV, and generally not more than 50 mV. EIS spectra are probably most valuable in assessing the recording capabilities of microelectrodes and, because the voltage excursions at the electrode are small, may also be a useful and benign method for the in vivo assessment of an electrode.

Impedance spectroscopy can be used to investigate both tissue and electrode properties. The resistive contribution of tissue conductivity to the overall electrode impedance is estimated from the impedance measured at high frequency, where the contribution to the impedance due to charge transfer at the electrode-tissue interface is negligible. This is shown in **Figure 9** in the Bode plots of impedance magnitude versus frequency for an AIROF microelectrode in PBS with three different NaCl concentrations (12.6, 126, and 252 mM, corresponding to ionic conductivities of 2.2, 12.1, and 24 mS cm^{-1}, respectively) but with the same buffer concentration. The high-frequency (10^5 Hz) impedance increases with decreasing electrolyte conductivity, whereas the low-frequency charge transfer impedance is unchanged. The opposite effect is observed with constant ionic conductivity but different buffer strength, as shown by the comparison in **Figure 10** of the same AIROF electrode in PBS and unbuffered NaCl. The high-frequency impedance is the same in both electrolytes, reflecting the same ionic conductivity, whereas the impedance at low frequency is higher in the unbuffered electrolyte due to the reduced availability of H^+ or OH^- as counterions.

The benefit of high-charge-capacity coatings in reducing the charge-transfer resistance of electrodes is shown by the Bode plots in **Figure 11** for smooth and porous TiN electrodes in a PBS electrolyte with identical shape and GSA. Both electrodes exhibit the same high-frequency impedance, whereas a marked reduction in low-frequency impedance is observed with the porous coating. Over a frequency range of 0.2–10^5 Hz, the porous film exhibits a near-resistive phase angle (approaching 0°) and an impedance modulus (|Z|) that is almost entirely solution resistance. A similar response is shown in **Figure 12** for SIROF-coated electrodes as a function of thickness of the SIROFs. It might be noted that the impedance of electroactive coatings can be a strong function of electrode potential. For example, both iridium oxide and PEDOT electrodes show

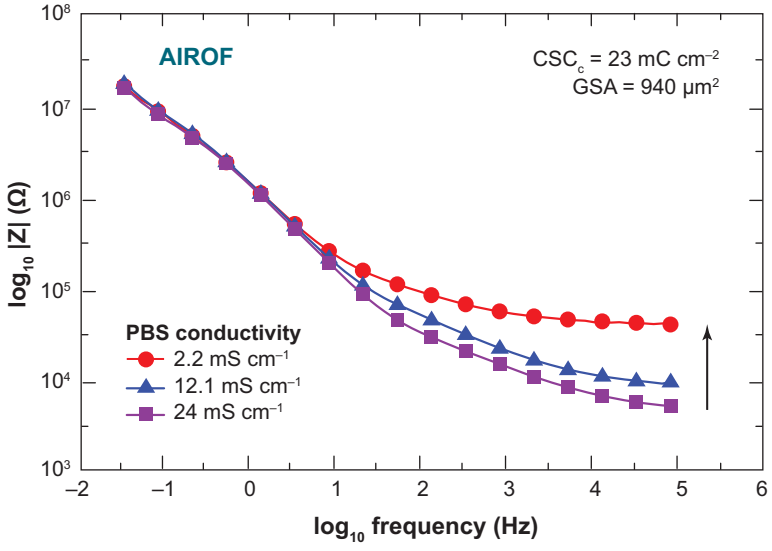

Figure 9

Impedance of an AIROF microelectrode (GSA = 940 μm^2) in three electrolytes of different ionic conductivities but fixed phosphate buffer concentration. The conductivities are determined by the NaCl concentrations of 12.6, 126, and 252 mM for the 2.2, 12.1 and 24 mS cm^{-1} conductivities, respectively.

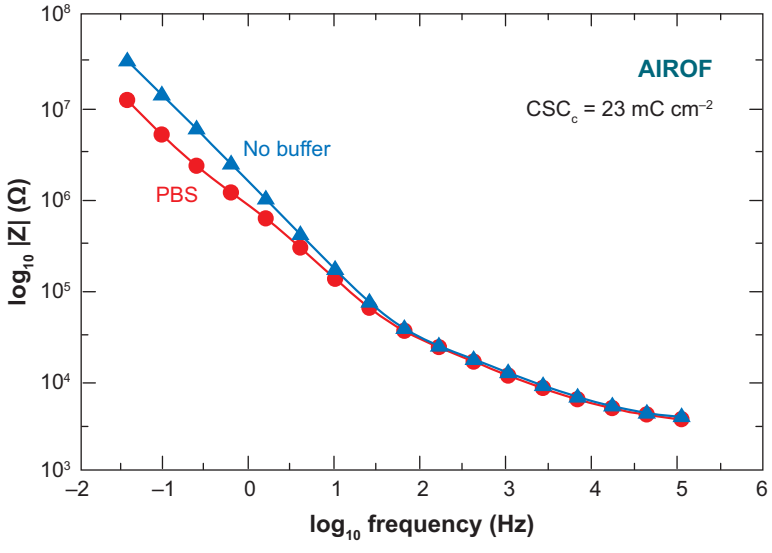

Figure 10

Impedance of an AIROF microelectrode (same as **Figure 9**) in PBS and unbuffered saline of similar ionic conductivities. The low-frequency charge-transfer impedance increases with decreasing buffer because of reduced availability of H^+ and OH^- counterions.

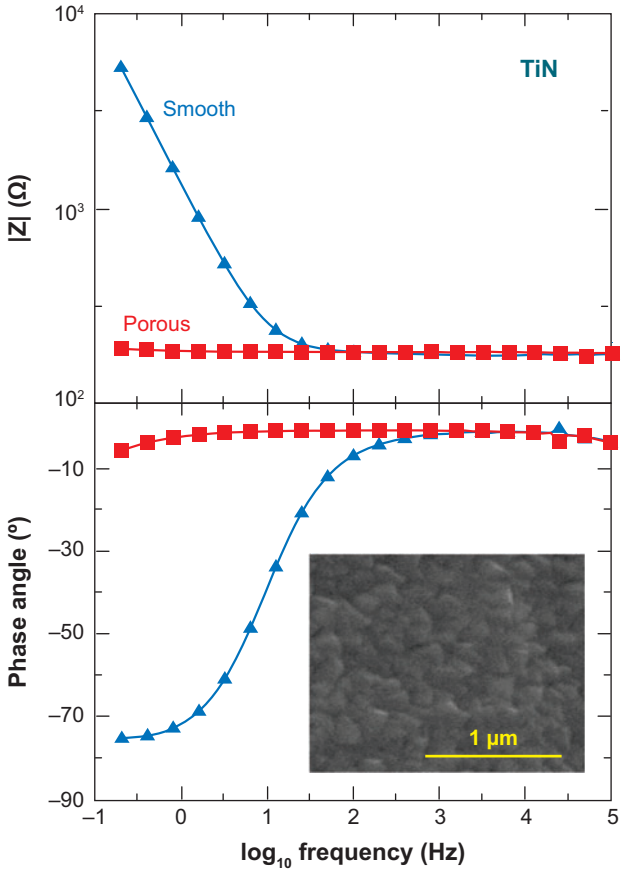

Figure 11

Comparison of the impedance of a smooth and porous TiN film demonstrating the reduction in impedance realized with a highly porous electrode coatings.

a large increase in impedance at negative potentials, below approximately −0.2 V (Ag|AgCl) for AIROF and −0.6 V (Ag|AgCl) for PEDOT. In the reduced state, both materials have low electronic conductivity, which is reflected in the impedance spectra. SIROF impedance is less sensitive to potential.

Voltage Transients

Voltage transient measurements are frequently used to estimate the maximum charge that can be injected in a current-controlled stimulation pulse. For in vitro measurements, the voltage transient is typically recorded in a three-electrode configuration using a large-area return electrode and a noncurrent-carrying reference electrode. The voltage transients are analyzed to determine the maximum polarization, both the most negative (E_{mc}) and most positive (E_{ma}), across the electrode-electrolyte interface. These potential extremes are then compared with established maximum potentials beyond which it is considered unsafe to polarize the electrode. Examples of maximum potential limits for typical stimulation electrode materials are provided in **Table 2**; these are typically water oxidation and reduction potentials.

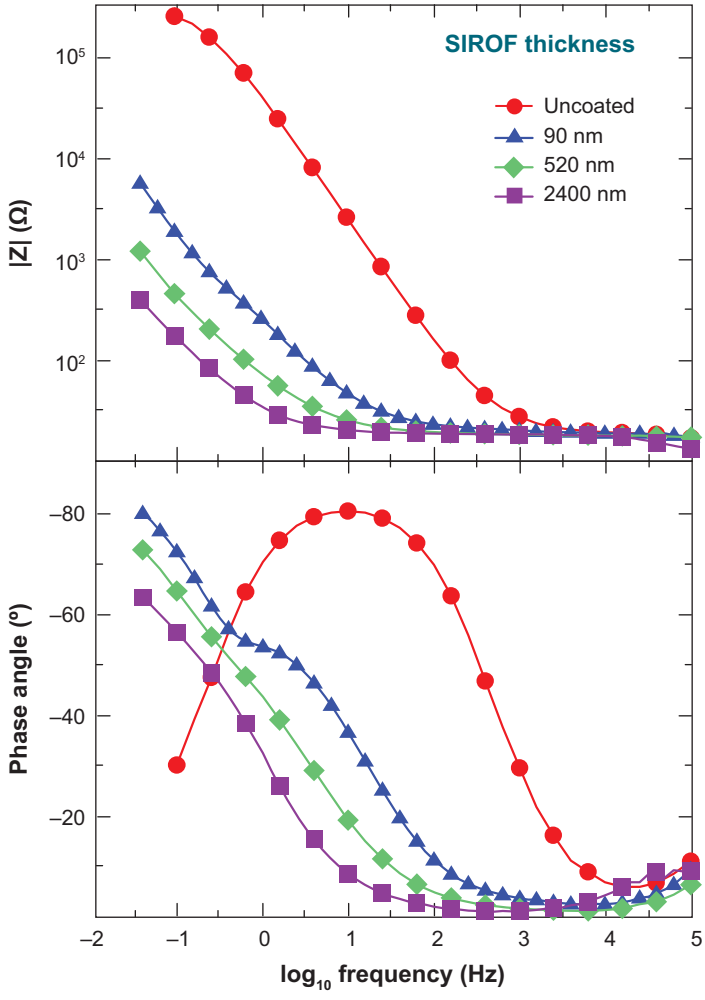

Figure 12

Impedance of SIROF coatings on PtIr macroelectrodes as a function of thickness.

An example of a voltage transient in response to a biphasic, symmetric current pulse is shown in **Figure 13**. There are several elements that contribute to the voltage transient, and these must be accounted for in the calculation of E_{mc} and E_{ma}. The contributing factors are the ohmic voltage drop (i_cR_i, R_i = electrolyte resistance) arising from the ionic conductivity of the electrolyte, the concentration overpotential (η_c), the activation overpotential (η_a), and the shift in the equilibrium potential of the electrode (ΔE_o) (see Activation Overpotential and Concentration Overpotential sidebars). The voltage transient is the sum of these,

$$\Delta V = i_cR_i + \eta_c + \eta_a + \Delta E_o, \quad (1)$$

where η_c, η_a, and ΔE_o have some time dependence. Only η_a and ΔE_o contribute to the polarization across the electrode-electrolyte interface (ΔE_p), and it is the ΔE_p relative to the potential of the electrode at the onset of the current pulse (the interpulse potential, E_{ipp}) that determines E_{mc} or

ACTIVATION OVERPOTENTIAL

The activation overpotential (η_a) is the voltage drop at the electrode-electrolyte interface necessary to maintain a net current flow when the current is provided by reduction or oxidation reactions. The current overpotential relationship is often described by the Butler-Volmer equation. Activation overpotential contributes to the driving force at the interface and can thus generate undesirable side reactions.

CONCENTRATION OVERPOTENTIAL

The transport of electroactive species—reactants or counterions—to an electrode in response to current flow creates a concentration gradient between the surface of the electrode and the bulk electrolyte. A voltage drop occurs in the electrolyte that is determined by the difference in equilibrium potential of the electrode reaction at the two concentration extremes. If, for example, the reduction of Ir oxide during a cathodal current pulse is governed by the reaction,

$$IrO_2 \cdot H_2O + e^- \Rightarrow IrO(OH) + OH^-,$$

the local pH change introduces a OH^- concentration gradient between the surface of the electrode and bulk electrolyte, resulting in a concentration overpotential (η_c). The magnitude of the overpotential can be estimated from the Nernst equation (117), which for the reaction above would indicate a 59 mV pH^{-1}-unit shift in potential as the pH adjacent to the Ir oxide changes. The pH changes during current pulsing can be significant, with a calculated extreme of pH = 11 during 0.2-ms cathodal pulsing (122) and a corresponding η_c of 0.24 V. For cathodal pulsing, the overpotential results in a more negative voltage transient.

E_{ma}. Thus, for a cathodal current pulse,

$$E_{mc} = E_{ipp} + \Delta E_p = E_{ipp} + (\Delta V - V_a), \quad (2)$$

where the access voltage V_a is taken as the near-instantaneous voltage change at either the onset of the current pulse or immediately after the current pulse is terminated. V_a can include overpotential terms as well as the electrolyte i_cR_i drop, and this introduces uncertainty into the value of ΔE_p. For example, with conical AIROF microelectrodes (**Figure 5**), the V_a measured from voltage transients is generally larger than the ohmic voltage drop in the electrolyte calculated using a spherical electrode approximation (117). The estimated i_cR_i in one study was typically 80% of the measured V_a, and as much as 20% of V_a may actually contribute to the potential drop across the interface (118). However, the approach to determining electrode polarization using V_a appears to predict electrode potentials fairly well based on the observation of electrode damage when exceeding water reduction potentials on AIROF (31) and correlations with potential-dependent impedance changes in AIROF and PEDOT. Charge-injection limits of Pt, PtIr, the Ir oxides, TiN, and PEDOT have all been determined using various voltage transient analysis methods.

There are additional considerations and limitations to the use of voltage transient measurements for determining charge-injection limits. First, the electrode's charge-injection capacity is highly dependent on current density, and measurements must be made at each current density of interest. This is shown in **Figure 14** for an AIROF microelectrode pulsed at 48 nC $phase^{-1}$ (2.4 mC cm^{-2}) at six different pulse widths corresponding to a current density range of 4.8 to 24 A cm^{-2}. The pulse waveform consists of a monophasic cathodal current pulse followed by an interphase period (i = 0) of 1.1 ms before the interpulse bias is reestablished. The E_{mc} varies from −0.11 V at 4.8 A cm^{-2} to −0.48 V at 24 A cm^{-2}, reflecting the larger activation overpotential at

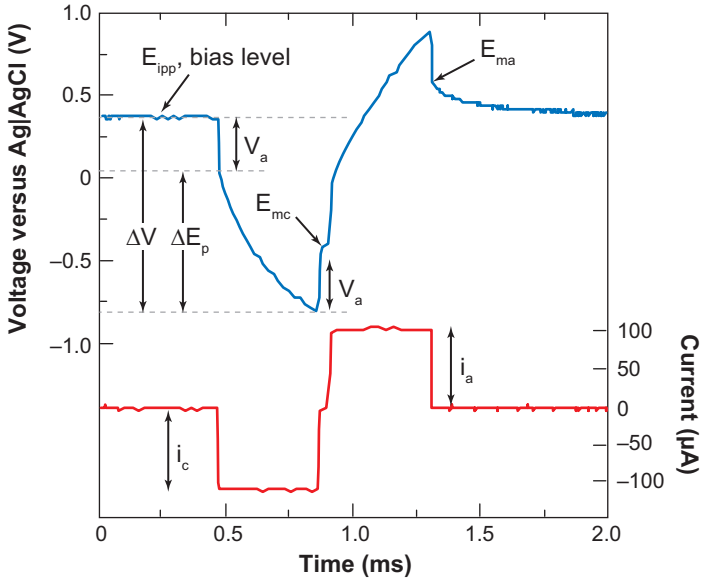

Figure 13

A voltage transient of an AIROF microelectrode in response to a biphasic, symmetric ($i_c = i_a$) current pulse.

the higher current density. A relevant observation from **Figure 14** is the behavior of the potential in the interphase region when $i = 0$. The AIROF was pulsed from a fixed E_{ipp} of 0.6 V, and the charge/phase was constant at each pulse width. Therefore, the equilibrium potential of the electrode (E_o), measured approximately 1.1 ms after the end of the pulse and before the anodic recharge back to E_{ipp}, should be nearly equal for all pulse widths, which it is ($E_o = 0.25$–0.28 V).

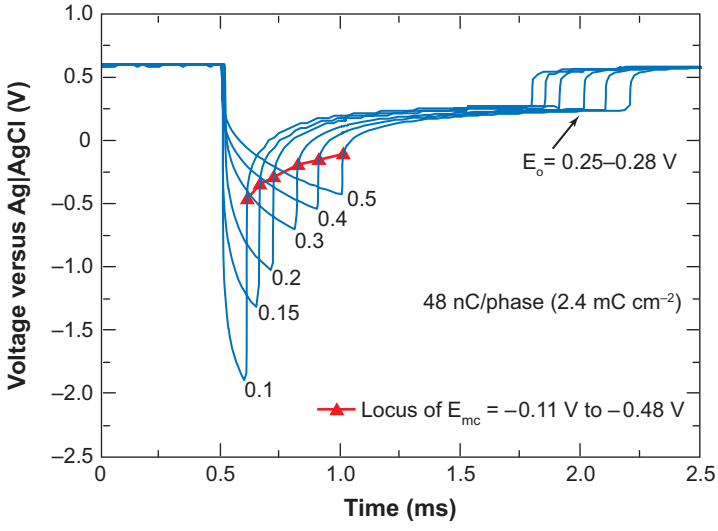

Figure 14

Comparison of voltage transients of an AIROF microelectrode pulsed at 48 nC phase^{-1} at pulsewidths from 0.1–0.5 ms.

If the E_o value were significantly different at different pulse widths, it would imply irreversibility in the charge-injection, presumably at the higher current densities.

An additional limitation of voltage transient measurements is the nonuniform current distribution that leads to larger potentials at the edge of disk-shaped electrodes and at the tips of conical penetrating electrodes. The potential measured with a distant reference electrode is an average across the surface of the stimulation electrode, and some regions of the stimulation electrode will be at a more extreme potential. For porous or three-dimensional electrodes, there is an additional nonuniformity in potential through the thickness of the electrode coating. Studies have shown that the nonuniform current and potential distributions can be quite large (119). An additional observation from **Figure 14** is that the electrode potential in the interphase period recovers from E_{mc} to E_o rapidly. This recovery is due to the internal equilibration of the nonuniformly reduced AIROF, which rapidly reaches a uniform potential (E_o) throughout film. In addition, counterion concentration gradients within the porous AIROF and the adjacent electrolyte dissipate as prepulse concentration levels are reestablished by diffusion. There is a corresponding change in the electrode potential (a concentration overpotential) that also contributes the potential shift in the interphase period.

A practical issue in determining E_{mc} or E_{ma} is the difficulty in accurately measuring V_a. Factors such as current-pulse rise times and stray capacitance can make identification of V_a difficult. An alternative strategy is to measure the potential excursion at the onset of the interphase period when $i = 0$, as shown in **Figure 13**. The latter approach has the advantage of accounting for changes in the ohmic resistance of the electrode during the course of a stimulation pulse. As noted previously, Ir oxide and PEDOT exhibit a potential-dependent increase in electronic resistance as the films are reduced. In **Figure 15**, V_a at the onset and end of a current pulse are shown for an AIROF microelectrode as a function of current and charge/phase. At a current of 200 μA, the initial and final V_a's deviate, with V_a at the end of the pulse becoming significantly larger, and it would be incorrect to use the initial rather than the final V_a in Equation 2 to calculate E_{mc}. The

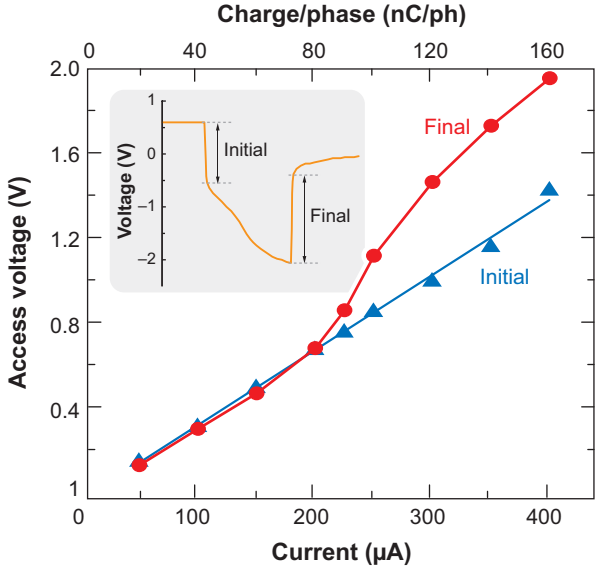

Figure 15

Comparison of the initial and final V_a for an AIROF microelectrode showing the large V_a at the end of the current pulse when the AIROF is reduced.

point of deviation corresponds to a calculated E_{mc} of approximately −0.2 V (Ag|AgCl), which is close to the potential at which AIROF transitions to the high-impedance state. The same behavior is observed for PEDOT, with a deviation occurring at −0.6 V, also corresponding to the onset of the high-impedance state.

Temperature effect. The ionic conductivity of an electrolyte and the rate constants of redox reactions at faradaic electrodes depend on temperature. Comparison of in vitro voltage transients of an AIROF microelectrode pulsed at 20°C and at 37°C in PBS revealed a decrease in R_a from 5360 Ω (20°C) to 4052 Ω at 37°C (calculated from the initial V_a). The electrode polarization under constant current pulsing was also reduced at the higher temperature, with a corresponding increase in charge injection capacity from 1.67 mC cm^{-2} at 20°C to 2.0 mC cm^{-2} at 37°C (0.1-ms pulse width). The dependence of Q_{inj} on temperature is significant and emphasizes the importance of testing at body temperature. Porous and multilayer electrodes, such as Ir oxide and porous TiN, are probably most sensitive to temperature effects because of transport limitations within these films.

Electrode size. Geometry and area affect charge-injection capacity measurements because of the nonuniform current distribution that localizes the charge-injection reactions to the perimeter or tip of an electrode. With short duration current pulses, the central regions of circular electrodes are underutilized and a lower overall maximum charge-injection density results. Area is also an important consideration because, as the electrode size is reduced, the electrode dimensions become smaller than the diffusion layer, the region around the electrode which deviates from bulk composition as current flows. For microelectrodes, the transport of counterions is facilitated by the small electrode size and reaction rates are less transport limited, with significantly higher charge-injection densities observed in voltage transient studies. This is shown in **Figure 16** for a series of SIROF electrodes with a range of GSAs from 1960 μm^2 to 125,600 μm^2. The SIROF is 200 nm thick and all the electrodes are on the same multielectrode array. The Q_{inj} of 5.3 mC cm^{-2} for the 1960-μm^2 microelectrode decreases to 1.7 mC cm^{-2} as the electrode size increases to 125,600 μm^2. These measurements emphasize the importance of electrode area in determining

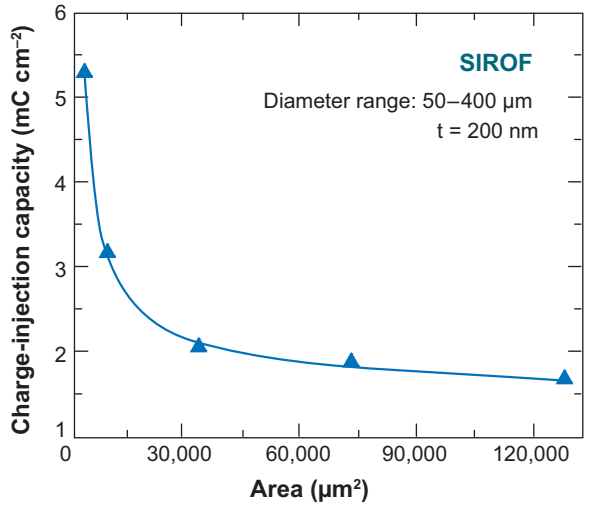

Figure 16

Charge-injection capacity as a function of electrode area. The importance of nonuniform current distributions and transport limitations in determining Q_{inj} are reflected in the area dependence.

the properties of stimulation electrodes, with the microelectrode (GSA = 1960 mm^2) exhibiting a factor of three higher Q_{inj} than the macroelectrode (125,600 μm^2) even though the SIROF coating is identical on both.

CHARGE INJECTION WAVEFORMS

This section discusses common strategies for providing stimulation waveforms. In all cases, the charge-balancing strategies can maintain the E_{ipp} of the electrode within a potential range that avoids electrode or tissue damage, but, as discussed above, this is a necessary but not sufficient condition for safe stimulation. Large potential excursions driven by high current densities during a pulse, including any charge-balancing second-phase pulses, can also be harmful to the electrode and tissue.

Monophasic Pulsing with Shorting to the Return Electrode

In stimulation devices employing a return electrode that is many times larger than the stimulation electrode, it is possible to short the stimulation and return electrodes in the interpulse period. This is the passively charge-balanced strategy described by Donaldson & Donaldson (88, 89). Because the return electrode is large, its potential does not change significantly with pulsing, and shorting poises the potential of the stimulation electrode to that of the return electrode in a manner analogous to a galvanic couple in which one electrode is nonpolarizable. This waveform is not necessarily balanced in the sense that the charge in the leading current pulse is equal in magnitude to the charge required to reestablish the poised potential. However, the stimulation electrode potential is always maintained between E_{mc} (for cathodal-first pulsing) and the return electrode potential, and, provided E_{mc} is within a safe operating range, the pulsing should not be harmful. A limitation of this strategy is the time required to reestablish the poised potential. If the pulse frequency is too high, there will be insufficient time between pulses to reestablish the potential, and significant and damaging polarization at the stimulation electrode may be encountered.

Monophasic Capacitor-Coupled Pulsing

With this waveform, charge is injected as a monophasic rectangular current pulse through a capacitor (**Figure 1*c***). After the initial pulse, the capacitor is discharged in the opposite direction using external switches that connect the capacitor across the stimulation and return electrodes. This strategy has been used extensively with intramuscular and peripheral nerve electrodes. Sometime after the capacitor discharge phase is complete, it is also possible to short together the stimulation and return electrodes.

Biphasic Current Waveforms

The use of current-controlled, biphasic waveforms having cathodal and anodal phases of equal charge/phase is common practice and, within the limits of pulse generators, ensures that the waveform is charge-balanced (**Figure 1*a***). It is also common practice with biphasic stimulators to use an isolation capacitor between the stimulator and electrode to prevent any net DC current flow. With the introduction of Ir oxide electrodes that require a positive potential bias to maximize charge-injection, this approach had to be modified because a small but continuous current flow is necessary in the interpulse period to sustain the bias. Typically, the bias is applied through a large isolation resistor connected between the electrode and the output side of the DC isolation

IMPLANTED REFERENCE ELECTRODES

A practical consideration when using an interpulse potential bias is the need for a reference electrode against which the bias is controlled. For in vitro studies, this electrode is usually a commercial Ag|AgCl or saturated calomel (SCE) reference electrode. In vivo, the use of a commercial reference electrode is not possible except in acute measurements where reference electrode contact may be established via the animal's tongue or other adequately conductive surface. For chronic studies, McCreery et al. (45) have employed an Ag|AgCl reference electrode fabricated from chloridized Ag wire encapsulated in slightly porous methyl methacrylate. In another approach, P. Troyk, S. Cogan, D. McCreery, M. Bak, Z. Hu, et al. (unpublished) have employed Pt wire as a reference electrode chronically for over four years in Macaque cortex. Although Pt is a polarizable electrode, observations have shown that Pt establishes a stable in vivo potential, on the order of 0 V versus Ag|AgCl (90).

capacitor. The use of charge-balanced asymmetric current waveforms has also been suggested by Cogan et al. (73) when using positively biased Ir oxide (**Figure 1*b***). The waveform retains overall zero net charge for the biphasic pulse, but employs an asymmetry in the current and pulse widths of each phase, with the second phase delivered at a lower current density for a longer period than the leading phase. This strategy minimizes positive polarization of the AIROF by the charge-balancing second phase and permits the use of a more positive bias for cathodal-first pulsing or a more negative bias for anodal-first pulsing to maximize charge injection. An optimum bias of 0.6 V (Ag|AgCl) was identified for cathodal-first pulsing of AIROF microelectrodes using a 1:4 (t_c:t_a) asymmetric waveform (73). It is possible to implement biased waveforms in both in vitro and chronic in vivo preparations (see Implanted Reference Electrodes sidebar).

Monophasic Current Pulses with Biased Waveforms

Monophasic current pulsing from a controlled interpulse bias was employed by Beebe & Rose (72) in their study of AIROF microelectrodes. The waveform is not truly monophasic because charge of the opposite sense to the stimulation pulse is injected when the interpulse bias is reestablished. As discussed above, the use of an interpulse bias requires a small net DC current to sustain a nonequilibrium state of the electrode (the biased state), so the overall waveform is not strictly charge-balanced. Although the use of a potential bias has the disadvantage of requiring a net DC current, it has the advantage of always establishing a fixed electrode potential in the interpulse period. The magnitude of the DC current necessary to sustain an electrode bias is quite small (see Maintaining an Electrode Bias sidebar). The transient portion of the waveform is thus

MAINTAINING AN ELECTRODE BIAS

To maintain a nonequilibrium potential with any practical electrode requires a net current flow across the electrode-tissue interface. The magnitude of this current is a consideration in the design of stimulator circuitry and for possible adverse reactions with tissue. Steady-state currents have been measured in vitro and in vivo as a function of bias. To maintain a 0.6 V bias (Ag|AgCl) required 3.4 $\mu A\ cm^{-2}$ in model-ISF and 7.7 $\mu A\ cm^{-2}$ in a subretinal implant of the same electrode, reflecting a difference in buffering capacity or additional oxidation of biomolecules at the in vivo electrode. The magnitude of the currents is quite small, typically <10 nA even for a relatively large 0.001 cm^2 AIROF electrode.

charge-balanced in the sense that the electrode potentials before and after a pulse are always equal. However, this does not mean necessarily that the cathodal and anodal charges are equal, and irreversible reactions and overpulsing of the electrode may still occur (31). In an effort to develop a stimulation strategy that is intrinsically safe, at least from the perspective of avoiding irreversible electrochemical reactions, Troyk et al. (116) proposed the use of compliance-voltage limited current pulsing. The current waveform is similar to that employed with biased, monophasic pulsing, except that the maximum compliance voltage (driving voltage) is preset to a value that prevents the voltage excursion of the stimulation electrode from exceeding a predetermined limit, selected to avoid electrode damage or water electrolysis.

Model-ISF: an inorganic model of interstitial fluid (ISF) comprising 2 mM Na_2HPO_4-$7H_2O$, 0.5 mM NaH_2PO_4-H_2O, 28 mM $NaHCO_3$, 7.5 mM $KHCO_3$, 110 mM NaCl, 0.5 mM $MgSO_4$, 0.5 mM $MgCl_2$, 0.5 mM $CaCl_2$ purged with 5% O_2, 6% CO_2, and 89% N_2

IN VITRO AND IN VIVO RESPONSE OF ELECTRODES

Most in vitro electrode characterization and long-term testing are carried out in an inorganic physiological saline, usually, but not always, with a buffer present, and often at ambient temperature. The in vivo environment presents important differences: (*a*) temperature, (*b*) the presence of organic species, (*c*) a tortuous diffusion path for charge carriers to the electrode, (*d*) the physiological response to a foreign body that results in the encapsulation of the electrode in a gliotic or fibrotic sheath, and (*e*) uncertain concentration of electrolytes and buffer, including carbon dioxide, near the surface of the electrode.

The most obvious difference in the in vitro and in vivo response of electrodes is the much larger driving voltages required to deliver stimulation pulses in vivo due to tissue resistance. A comparison of AIROF macroelectrodes (GSA = 125,600 μm^2) pulsed in model-ISF and subretinally in rabbit demonstrated the need for a factor-of-three-higher driving voltage in vivo to deliver the same charge/phase, as shown in **Figure 17** (120). Similarly, Hu et al. (121) observed a factor of four decrease in the in vivo charge/phase with AIROF microelectrodes when comparing compliance limited pulsing in dilute phosphate buffered saline and the brain of zebra finch. Perhaps more importantly, electrode polarization (ΔE_p) also appears to be greater in vivo, being approximately a

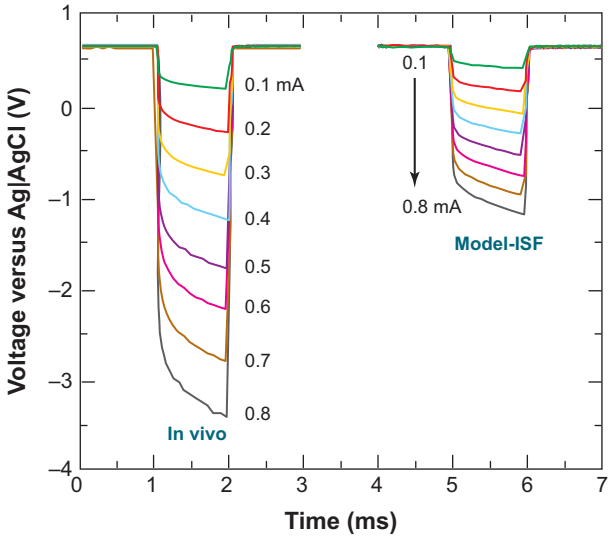

Figure 17

Comparison of in vivo and in vitro voltage transients of an AIROF electrode pulsed in an inorganic model of interstitial fluid (model-ISF) and subretinally in rabbit.

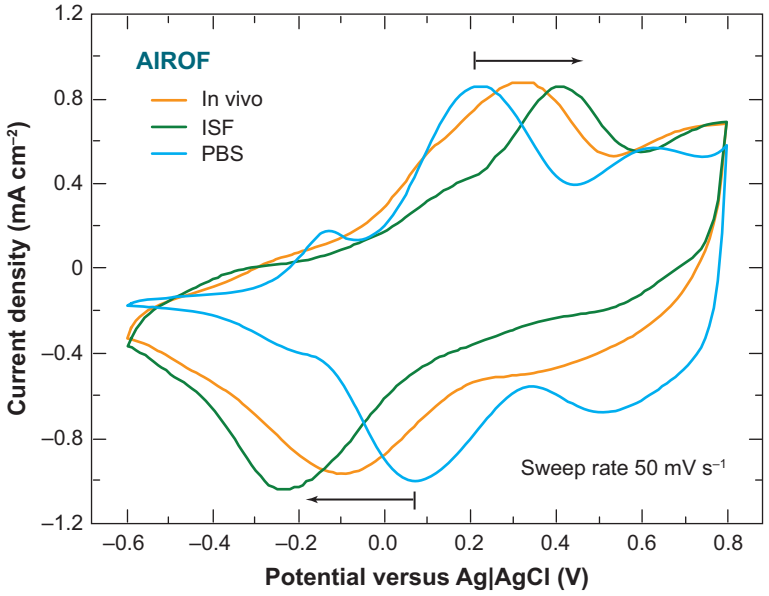

Figure 18

Comparison of the CV response of an AIROF electrode in PBS, model-ISF, and subretinally in rabbit.

factor of two higher for the same level of charge/phase in the study by Cogan (120). Two possible reasons for the higher in vivo polarization are biomolecule absorption and reduced counterion transport in the tissue immediately adjacent to the electrode. The rate of counterion transport is equal to the current during a stimulation pulse, and if the current exceeds the rate at which counterions for the intended reversible processes are transported to or from the electrode, the electrode will be polarized until another, possibly irreversible, reaction is recruited to maintain

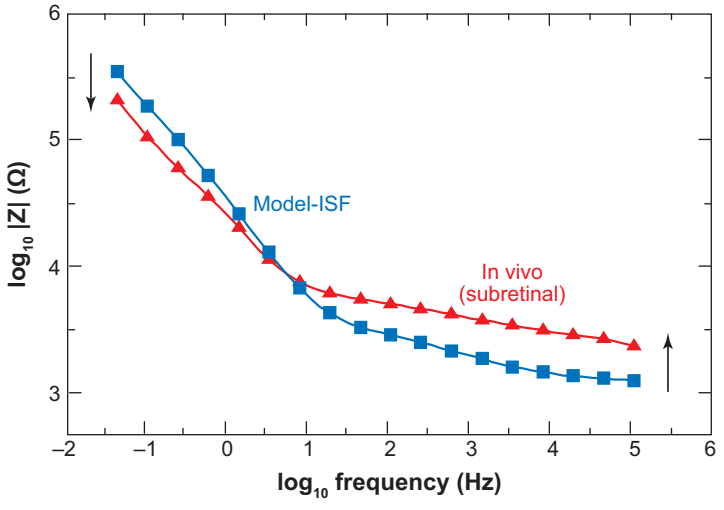

Figure 19

Comparison of the impedance magnitude of an AIROF electrode in model-ISF and subretinally in rabbit.

the current. Obviously, Q_{inj} obtained from in vitro measurements cannot be employed in vivo without caution.

Comparison of the CV response of electrodes in vitro and in vivo is also revealing. In **Figure 18**, three CVs of an AIROF electrode are compared in PBS, model-ISF, and subretinally in rabbit. The interesting observation is that the shift in the peak potentials of the Ir^{3+}/Ir^{4+} redox wave (indicated by the arrows) from that obtained in highly buffered PBS is less in vivo than in the model-ISF. This suggests that the in vivo buffering capacity is intermediate between that of model-ISF and PBS and that the Ir^{3+}/Ir^{4+} redox reaction is more facile in vivo than in model-ISF. This observation is supported by a comparison of in vivo and in vitro impedance spectra, shown in **Figure 19**, for an AIROF electrode in model-ISF and subretinally in rabbit. In vivo, the impedance magnitude is larger at higher frequency, reflecting the increased contribution from tissue resistance, whereas at low frequency the in vivo impedance is reduced, presumably due to the greater availability of H^+ or OH^- counterions compared with model-ISF.

CONCLUSIONS

The trend in neural prostheses and electrical stimulation therapies is toward systems having a large number of electrodes that each provide focal stimulation of a small volume of neural tissue and permit the recording of action potentials from single neurons or from small populations of neurons. The use of adaptive prostheses that modulate or initiate stimulation in response to recorded neural signals is also contemplated. Electrode materials for these prostheses have been identified, and their in vitro electrochemical properties relevant to stimulation and recording, as measured in model physiological electrolytes, are generally appropriate for their intended use. However, chronic studies reveal a more complicated situation in which electrode performance and properties vary over time. It is often not clear whether these variations are due to changes in the tissue encapsulating the electrode, degradation of electrode materials, or whether there is a change in the excitability or functional response of the neural tissue.

FUTURE DIRECTIONS

The development of microelectrode-based neural prostheses would benefit from future studies in several areas, including the following:

1. The development of in vivo, nondestructive methods to diagnose the condition of implanted microelectrodes and to identify factors that contribute to temporal changes in electrode properties.
2. The development of techniques to maintain or rejuvenate the low-impedance properties of recording microelectrodes without causing tissue damage. For example, the use of a sustained positive voltage bias reduces the impedance and recovers the recording properties of microelectrodes, but the improvement is temporary and tissue damage is likely with repeated applications of the bias (54). Other less damaging protocols might be developed that sustain a low-impedance state chronically.
3. For stimulation, methods of charge-injection that limit the polarization of an electrode to within safe electrochemical limits that avoid damage to electrodes and tissue are also desirable. However, in view of the high driving voltages required to overcome tissue impedance during stimulation, it is not certain that intrinsically safe charge-injection protocols can be developed other than through extensive in vivo testing.

4. In vivo measurement of the charge-injection limits of electrodes and how these limits change with time following implantation.
5. A recent and potentially important approach to improving the performance and stability of stimulation and recording microelectrodes is the use of biologically inspired electrode treatments and coatings that moderate adverse tissue responses or enhance the functional performance of electrodes.

DISCLOSURE STATEMENT

S.C. is an employee of EIC Laboratories, a for-profit company active in medical electrode coating technology development.

ACKNOWLEDGMENTS

The insight and contributions of Dr. Philip Troyk at the Illinois Institute of Technology and Dr. Douglas McCreery at the Huntington Medical Research Institutes through several collaborations and many discussions are gratefully acknowledged. Gratitude is extended to Dr. Joseph Rizzo at the Boston VA Hospital and Massachusetts Eye and Ear Infirmary for the opportunity to investigate the properties of electrodes in subretinal implants. Electrode data were acquired during the course of studies supported by the National Institutes of Health (Dr. Troyk, NIH No. R01 EB002184-02; Dr. McCreery, NINDS No. R01NS054121) and the Department of Veterans Affairs, Research Rehabilitation and Development Service (Dr. Rizzo, Grant No. C4266-C). The work was supported in part at EIC Laboratories under NIH Grants No. R44 NS039714-03 and No. 2R44NS049687-02.

LITERATURE CITED

1. Li Y, Mogul DJ. 2007. Electrical control of epileptic seizures. *J. Clin. Neurophysiol.* 24:197–204
2. Normann RA. 2007. Technology insight: future neuroprosthetic therapies for disorders of the nervous system. *Nat. Clin. Pract. Neurol.* 3:444–52
3. Perlmutter JS, Mink JW. 2006. Deep brain stimulation. *Annu. Rev. Neurosci.* 29:229–57
4. Clark GM. 2006. The multiple-channel cochlear implant: the interface between sound and the central nervous system for hearing, speech, and language in deaf people—a personal perspective. *Phil. Trans. R. Soc. London B* 361:791–810
5. Shepherd RK, McCreery DB. 2006. Basis of electrical stimulation of the cochlea and the cochlear nucleus. *Adv. Otorhinolaryngol.* 64:186–205
6. Jackson A, Moritz CT, Mavoori J, Lucas TH, Fetz EE. 2006. The Neurochip BCI: towards a neural prosthesis for upper limb function. *IEEE Trans. Neural Syst. Rehabil. Eng.* 14:187–90
7. Rutten WL. 2002. Selective electrical interfaces with the nervous system. *Annu. Rev. Biomed. Eng.* 4:407–52
8. Jezernik S, Craggs M, Grill WM, Creasey G, Rijkhoff NJ. 2002. Electrical stimulation for the treatment of bladder dysfunction: current status and future possibilities. *Neurol. Res.* 24:413–30
9. Prochazka A, Mushahwar VK, McCreery BB. 2001. Neural prostheses. *J. Physiol.* 533:99–109
10. Hoffer JA, Stein RB, Haugland MK, Sinkjaer T, Durfee WK, et al. 1996. Neural signals for command control and feedback in functional neuromuscular stimulation: a review. *J. Rehabil. Res. Dev.* 33:145–57
11. Loeb GE. 1989. Neural prosthetic interfaces with the nervous system. *Trends Neurosci.* 12:195–201
12. Tehovnik EJ, Tolias AS, Sultan F, Slocum WM, Logothetis NK. 2006. Direct and indirect activation of cortical neurons by electrical microstimulation. *J. Neurophysiol.* 96:512–21

13. Tehovnik EJ. 1996. Electrical stimulation of neural tissue to evoke behavioral responses. *J. Neurosci. Methods* 65:1–17
14. McIntyre CC, Grill WM. 2000. Selective microstimulation of central nervous system neurons. *Ann. Biomed. Eng.* 28:219–33
15. Basser PJ, Roth BJ. 2000. New currents in electrical stimulation of excitable tissues. *Annu. Rev. Biomed. Eng.* 2:377–97
16. Lebedev MA, Nicolelis MA. 2006. Brain-machine interfaces: past, present and future. *Trends Neurosci.* 29:536–46
17. Friehs GM, Zerris VA, Ojakangas CL, Fellows MR, Donoghue JP. 2004. Brain-machine and brain-computer interfaces. *Stroke* 35:2702–5
18. Donoghue JP. 2002. Connecting cortex to machine: recent advances in brain interfaces. *Nat. Neurosci.* 5:1085–88
19. Merrill DR, Bikson, Jefferys JGR. 2005. Electrical stimulation of excitable tissue: design of efficacious and safe protocols. *J. Neurosci. Methods* 141:171–98
20. Robblee LS, Rose TL. 1990. Electrochemical guidelines for selection of protocols and electrode materials for neural stimulation. In *Neural Prostheses: Fundamental Studies*, ed. WF Agnew, DB McCreery, pp. 25–66. Englewood Cliffs, NJ: Prentice Hall
21. Polikov VS, Tresco PA, Reichert WM. 2005. Response of brain tissue to chronically implanted neural electrodes. *J. Neurosci. Methods* 148:1–18
22. Twardoch UM. 1994. Integrity of ultramicro-stimulation electrodes determined from electrochemical measurements. *J. Appl. Electrochem.* 24:835–57
23. Fang ZP, Mortimer JT. 1991. Selective activation of small motor axons by quasi-trapezoidal current pulses. *IEEE Trans. Biomed. Eng.* 38:168–74
24. McIntyre CC, Grill WM. 2002. Extracellular stimulation of central neurons: influence of stimulus waveform and frequency on neuronal output. *J. Neurophysiol.* 88:1592–604
25. Jensen RJ, Rizzo JF. 2007. Thresholds for activation of rabbit retinal ganglion cells with a subretinal electrode. *Exp. Eye Res.* 83:367–73
26. Scheiner A, Mortimer JT, Roessmann U. 1990. Imbalanced biphasic electrical stimulation: muscle tissue damage. *Ann. Biomed. Eng.* 18:407–25
27. McHardy J, Geller D, Brummer SB. 1977. An approach to corrosion control during electrical stimulation. *Ann. Biomed. Eng.* 5:144–49
28. Brummer SB, Turner MJ. 1977. Electrochemical considerations for safe electrical stimulation of the nervous system with platinum electrodes. *IEEE Trans. Biomed. Eng.* 24:59–63
29. Agnew WF, Yuen TG, McCreery DB, Bullara LA. 1986. Histopathologic evaluation of prolonged intracortical electrical stimulation. *Exp. Neurol.* 92:162–85
30. Robblee LS, McHardy J, Agnew WF, Bullara LA. 1983. Electrical stimulation with Pt electrodes. VII. Dissolution of Pt electrodes during electrical stimulation of the cat cerebral cortex. *J. Neurosci. Methods* 9:301–8
31. Cogan SF, Guzelian AA, Agnew WF, Yuen TGH, McCreery DB. 2004. Over-pulsing degrades activated iridium oxide films used for intracortical neural stimulation. *J. Neurosci. Methods* 137:141–50
32. Mahadevappa M, Weiland JD, Yanai D, Fine I, Greenberg RJ, Humayun MS. 2005. Perceptual thresholds and electrode impedance in three retinal prosthesis subjects. *IEEE Trans. Neural Syst. Rehabil. Eng.* 13:201–6
33. Rizzo JF, Wyatt J, Loewenstein J, Kelly S, Shire D. 2003. Perceptual efficacy of electrical stimulation of human retina with a microelectrode array during short-term surgical trials. *Invest. Ophthalmol. Vis. Sci.* 44:5362–69
34. Veraart C, Raftopoulos C, Mortimer JT, Delbeke J, Pins D, et al. 1998. Visual sensations produced by optic nerve stimulation using an implanted self-sizing spiral cuff electrode. *Brain Res.* 813:181–86
35. Hambrecht FT. 1995. Visual prostheses based on direct interfaces with the visual system. *Bulliere's Clin. Neurol.* 4:147–65
36. McCreery DB, Shannon RV, Moore JK, Chatterjee M. 1998. Accessing the tonotopic organization of the ventral cochlear nucleus by intranuclear microstimulation. *IEEE Trans. Rehabil. Eng.* 6:391–99

37. McCreery DB, Yuen TG, Bullara LA. 2000. Chronic microstimulation in the feline ventral cochlear nucleus: physiologic and histologic effects. *Hear. Res.* 149:223–38
38. Shannon RV, Otto SR. 1990. Psychophysical measures from electrical stimulation of the human cochlear nucleus. *Hear. Res.* 47:159–68
39. Grill WM, Bhadra N, Wang B. 1999. Bladder and urethral pressures evoked by microstimulation of the sacral spinal cord in cats. *Brain Res.* 836:19–30
40. Kuncel AM, Grill WM. 2004. Selection of stimulus parameters for deep brain stimulation. *Clin. Neurophysiol.* 115:2431–41
41. Nannini N, Horch K. 1991. Muscle recruitment with intrafascicular electrodes. *IEEE Trans. Biomed. Eng.* 38:769–76
42. Branner A, Stein RB, Normann RA. 2001. Selective stimulation of cat sciatic nerve using an array of varying-length microelectrodes. *J. Neurophysiol.* 85:1585–94
43. McCreery DB, Agnew WF, Yuen TG, Bullara L. 1990. Charge density and charge per phase as cofactors in neural injury induced by electrical stimulation. *IEEE Trans. Biomed. Eng.* 37:996–1001
44. McCreery DB, Yuen TG, Agnew WF, Bullara LA. 1994. Stimulus parameters affecting tissue injury during microstimulation in the cochlear nucleus of the cat. *Hear Res.* 77:105–15
45. McCreery DB, Agnew WF, Bullara LA. 2002. The effects of prolonged intracortical microstimulation on the excitability of pyramidal tract neurons in the cat. *Ann. Biomed. Eng.* 30:107–19
46. Donoghue JP, Nurmikko A, Black M, Hochberg LR. 2007. Assistive technology and robotic control using motor cortex ensemble-based neural interface systems in humans with tetraplegia. *J. Physiol.* 579:603–11
47. McCreery D, Lossinsky A, Pikov V, Liu X. 2006. Microelectrode array for chronic deep-brain microstimulation and recording. *IEEE Trans. Biomed. Eng.* 53:726–37
48. Gluckman BJ, Nguyen H, Weinstein SL, Schiff SJ. 2001. Adaptive electric field control of epileptic seizures. *J. Neurosci.* 21:590–600
49. Rousche PJ, Normann RA. 1998. Chronic recording capability of the Utah Intracortical Electrode Array in cat sensory cortex. *J. Neurosci. Methods* 82:1–15
50. Nicolelis MA, Dimitrov D, Carmena JM, Crist R, Lehew G, et al. 2003. Chronic, multisite, multielectrode recordings in macaque monkeys. *Proc. Natl. Acad. Sci. USA* 100:11041–46
51. Vetter RJ, Williams JC, Hetke JF, Nunamaker EA, Kipke DR. 2004. Chronic neural recording using silicon-substrate microelectrode arrays implanted in cerebral cortex. *IEEE Trans. Biomed. Eng.* 51:896–904
52. Suner S, Fellows MR, Vargas-Irwin C, Nakata GK, Donoghue JP. 2005. Reliability of signals from a chronically implanted, silicon-based electrode array in nonhuman primate motor cortex. *IEEE Trans. Neural Syst. Rehabil. Eng.* 13:525–41
53. Robinson DA. 1968. The electrical properties of metal microelectrodes. *Proc. IEEE* 56:1065–1071
54. Johnson MD, Otto KJ, Kipke DR. 2005. Repeated voltage biasing improves unit recordings by reducing resistive tissue impedances. *IEEE Trans. Neural Syst. Rehab. Eng.* 13:160–65
55. Edell DJ, Toi VV, McNeil, Clark LD. 1992. Factors influencing the biocompatibility of insertable silicon microshafts in cerebral cortex. *IEEE Trans. Biomed. Eng.* 39:635–43
56. Turner N, Shain W, Szarowski DH, Andersen M, Martins S, et al. 1999. Cerebral astrocyte response to micromachined silicon implants. *Exp. Neurol.* 156:33–49
57. Szarowski DH, Andersen MD, Retterer S, Spence AJ, Isaacson M, et al. 2003. Brain responses to micromachined silicon devices. *Brain Res.* 983:23–35
58. Biran R, Martin DC, Tresco PA. 2005. Neuronal cell loss accompanies the brain tissue response to chronically implanted silicon microelectrode arrays. *Exp. Neurol.* 195:115–26
59. Niparko JK, Altschuler RA, Xue X, Wiler JA, Anderson DJ. 1989. Surgical implantation and biocompatibility of central nervous system auditory prostheses. *Ann. Otol. Rhinol. Laryngol.* 98:965–70
60. Kim Y-T, Hitchcock RW, Bridge MJ, Tresco PA. 2004. Chronic response of adult rat brain tissue to implants anchored to the skull. *Biomaterials* 25:2229–37
61. Merrill DR, Tresco PA. 2005. Impedance characterization of microarray recording electrodes in vitro. *IEEE Trans. Biomed. Eng.* 52:1960–65
62. Carmena JM, Lebedev MA, Henriquez CS, Nicolelis MA. 2005. Stable ensemble performance with single-neuron variability during reaching movements in primates. *J. Neurosci.* 25:10712–16

63. Supèr H, Roelfsema PR. 2005. Chronic multiunit recordings in behaving animals: advantages and limitations. *Prog. Brain Res.* 147:263–82
64. Kennedy PR, Mirra SS, Bakay RA. 1992. The cone electrode: ultrastructural studies following long-term recording in rat and monkey cortex. *Neurosci. Lett.* 142:89–94
65. Kennedy PR. 1989. The cone electrode: a long-term electrode that records from neurites grown onto its recording surface. *J. Neurosci. Methods* 29:181–93
66. Kennedy PR, Kirby MT, Moore MM, King B, Mallory A. 2004. Computer control using human intracortical local field potentials. *IEEE Trans. Neural. Syst. Rehabil. Eng.* 12:339–44
67. He W, Bellamkonda RV. 2005. Nanoscale neuro-integrative coatings for neural implants. *Biomaterials* 26:2983–90
68. Pettingill LN, Richardson RT, Wise AK, O'Leary SJ, Shepherd RK. 2007. Neurotrophic factors and neural prostheses: potential clinical applications based upon findings in the auditory system. *IEEE Trans. Biomed. Eng.* 54:1138–48
69. Winter JO, Cogan SF, Rizzo JF. 2007. Neurotrophin-eluting hydrogel coatings for neural stimulating electrodes. *J. Biomed. Mater. Res. B Appl. Biomater.* 81:551–63
70. Conway BE. 1991. Transition from "supercapacitor" to "battery" behavior in electrochemical energy storage. *J. Electrochem. Soc.* 138:1539–48
71. Rose TL, Robblee LS. 1990. Electrical stimulation with Pt electrodes. VII. Electrochemically safe charge injection limits with 0.2 ms pulses. *IEEE Trans. Biomed. Eng.* 37:1119–20
72. Beebe X, Rose TL. 1988. Charge injection limits of activated iridium oxide electrodes with 0.2 ms pulses in bicarbonate buffered saline. *IEEE Trans. Biomed. Eng.* 35:494–95
73. Cogan SF, Troyk PR, Ehrlich J, Plante TD, Detlefsen DE. 2006. Potential-biased, asymmetric waveforms for charge-injection with activated iridium oxide (AIROF) neural stimulation electrodes. *IEEE Trans Biomed Eng.* 53:327–32
74. Robblee LS, Mangaudis MJ, Lasinsky ED, Kimball AG, Brummer SB. 1986. Charge injection properties of thermally-prepared iridium oxide films. *Mat. Res. Soc. Symp. Proc.* 55:303–10
75. Cogan SF, Plante TD, Ehrlich J. 2004. Sputtered iridium oxide films (SIROFs) for low-impedance neural stimulation and recording electrodes. *Proc. IEEE. Eng. Med. Biol. Soc.* 6:4153–56
76. Rose TL, Kelliher EM, Robblee LS. 1985. Assessment of capacitor electrodes for intracortical neural stimulation. *J. Neurosci. Methods* 12:181–93
77. Schmidt EM, Hambrecht FT, McIntosh JS. 1982. Intracortical capacitor electrodes: preliminary evaluation. *J. Neurosci. Methods* 5:33–39
78. Weiland JD, Anderson DJ, Humayun MS. 2002. In vitro electrical properties for iridium oxide versus titanium nitride stimulating electrodes. *IEEE Trans. Biomed. Eng.* 49:1574–79
79. Cogan SF, Peramunage D, Smirnov A, Ehrlich J, McCreery DB, Manoonkitiwongsa PS. 2007. Polyethylenedioxythiophene (PEDOT) coatings for neural stimulation and recording electrodes. *Mater. Res. Soc. Meet.*, Boston, Nov. 26–30 (Abstr. QQ2.7)
80. Guyton DL, Hambrecht FT. 1974. Theory and design of capacitor electrodes for chronic stimulation. *Med. Biol. Eng.* 12:613–20
81. Schaldach M, Hubmann M, Weikl A, Hardt R. 1990. Sputter-deposited TiN electrode coatings for superior sensing and pacing performance. *Pacing Clin. Electrophysiol.* 13:1891–95
82. Norlin A, Pan J, Leygraf C. 2005. Investigation of electrochemical behavior of stimulation/sensing materials for pacemaker electrode applications. *J. Electrochem. Soc.* 152:J7–15
83. Posey FA, Morozumi T. 1966. Theory of potentiostatic and galvanostatic charging of the double layer in porous electrodes. *J. Electrochem. Soc.* 113:176–84
84. Goldberg IB, Bard AJ. 1972. Resistive effects in thin electrochemical cells: digital simulations of current and potential steps in thin layer electrochemical cells. *J. Electroanal. Chem.* 38:313–22
85. Dupont AC, Bagg SD, Baker L, Creasy JL, Romano C, et al. 2004. First patients with BION implants for therapeutic electrical stimulation. *Neuromodulation* 7:38–47
86. Loeb GE, Peck RA, Moore WH, Hood K. 2001. BION system for distributed neural prosthetic interfaces. *Med. Eng. Phys.* 23:9–18

87. Cogan SF, Troyk PR, Ehrlich J, Plante TD. 2005. In vitro comparison of the charge-injection limits of activated iridium oxide (AIROF) and platinum-iridium microelectrodes. *IEEE Trans. Biomed. Eng.* 52:1612–14
88. Donaldson ND, Donaldson PE. 1986. When are actively balanced biphasic ('Lilly') stimulating pulses necessary in a neurological prosthesis? I. Historical background; Pt resting potential; Q studies. *Med. Biol. Eng. Comput.* 24:41–49
89. Donaldson ND, Donaldson PE. 1986. When are actively balanced biphasic ('Lilly') stimulating pulses necessary in a neurological prosthesis? II. pH changes; noxious products; electrode corrosion; discussion. *Med. Biol. Eng. Comput.* 24:50–56
90. Craggs MD, Donaldson NN, Donaldson PE. 1986. Performance of platinum stimulating electrodes, mapped on the limit-voltage plane. Part 1. Charge injection in vivo. *Med. Biol. Eng. Comput.* 24:424–30
91. Robblee LS, McHardy J, Marston JM, Brummer SB. 1980. Electrical stimulation with Pt electrodes. V. The effect of protein on Pt dissolution. *Biomaterials* 1:135–39
92. Hibbert DB, Weitzner K, Tabor B, Carter P. 2000. Mass changes and dissolution of platinum during electrical stimulation in artificial perilymph. *Biomaterials* 21:2177–82
93. Tykocinski M, Duan Y, Tabor B, Cowan RS. 2001. Chronic electrical stimulation of the auditory nerve using high surface area (HiQ) platinum electrodes. *Hear. Res.* 159:53–68
94. Zhou DM. 2005. *U.S. Patent No. 6,974,533*
95. Robblee LS, Lefko JL, Brummer SB. 1983. Activated Ir: an electrode suitable for reversible charge injection in saline. *J. Electrochem. Soc.* 130:731–33
96. Mozota J, Conway BE. 1983. Surface and bulk processes at oxidized iridium electrodes—I. Monolayer stage and transition to reversible multilayer oxide film behavior. *Electrochim. Acta* 28:1–8
97. McCreery DB, Bullara LA, Agnew WF. 1986. Neuronal activity evoked by chronically implanted intracortical microelectrodes. *Exp. Neur.* 92:147–61
98. Anderson DJ, Najafi K, Tanghe SJ, Evans DA, Levy KL, et al. 1989. Batch-fabricated thin-film electrodes for stimulation of the central auditory system. *IEEE Trans. Biomed. Eng.* 36:693–704
99. Schmidt EM, Bak MJ, Hambrecht FT, Kufta CV, O'Rourke DK, Vallabhanath P. 1996. Feasibility of a visual prosthesis for the blind based on intracortical microstimulation of the visual cortex. *Brain* 119:507–22
100. Klein JD, Clauson SL, Cogan SF. 1989. Morphology and charge capacity of sputtered iridium oxide films. *J. Vac. Sci. Technol.* A7:3043–47
101. Slavcheva E, Vitushinsky R, Mokwa W, Schnakenberg U. 2004. Sputtered iridium oxide films as charge injection material for functionalized electrostimulation. *J. Electrochem. Soc.* 151:E226–37
102. Wessling B, Mokwa W, Schnakenberg U. 2006. RF-sputtering of iridium oxide to be used as stimulation material in functional medical implants. *J. Micromech. Microeng.* 16:S142–48
103. Foos JS, Erker SM. 1986. Rate enhancement in modified polypyrrole electrodes. *J. Electrochem. Soc.* 133:1983–84
104. Cui X, Lee VA, Raphael Y, Wiler JA, Hetke JF, et al. 2001. Surface modification of neural recording electrodes with conducting polymer/biomolecule blends. *J. Biomed. Mater. Res.* 56:261–72
105. Cui X, Wiler J, Dzaman M, Altschuler RA, Martin DC. 2003. In vivo studies of polypyrrole/peptide coated neural probes. *Biomaterials* 24:777–87
106. Cui X, Martin DC. 2003. Electrochemical deposition and characterization of poly(3,4-ethylenedioxythiophene) on neural microelectrode arrays. *Sens. Actuators B* 89:92–102
107. Ludwig KA, Uram JD, Yang J, Martin DC, Kipke DR. 2006. Chronic neural recordings using silicon microelectrode arrays electrochemically deposited with a poly(3,4-ethylenedioxythiophene) (PEDOT) film. *J. Neural. Eng.* 3:59–70
108. Xiao Y, Cui X, Hancock JM, Bouguettaya M, Reynolds JR, Martin DC. 2004. Electrochemical polymerization of poly(hydroxymethylated-3,4-ethylenedioxythiophene) (PEDOT-MeOH) on multichannel neural probes. *Sens. Actuators B* 99:437–43
109. Richardson-Burns SM, Hendricks JL, Martin DC. 2007. Electrochemical polymerization of conducting polymers in living neural tissue. *J. Neural. Eng.* 4:L6–13

110. Richardson-Burns SM, Hendricks JL, Foster B, Povlich LK, Kim DH, Martin DC. 2007. Polymerization of the conducting polymer poly(3,4-ethylenedioxythiophene) (PEDOT) around living neural cells. *Biomaterials* 28:1539–52
111. Nyberg T, Shimada A, Torimitsu K. 2007. Ion conducting polymer microelectrodes for interfacing with neural networks. *J. Neurosci. Methods* 160:16–25
112. Wang K, Fishman HA, Dai H, Harris JS. 2006. Neural stimulation with a carbon nanotube microelectrode array. *Nano Lett.* 6:2043–48
113. Nguyen-Vu TD, Chen H, Cassell AM, Andrews RJ, Meyyappan M, Li J. 2007. Vertically aligned carbon nanofiber architecture as a multifunctional 3-D neural electrical interface. *IEEE Trans. Biomed. Eng.* 54:1121–28
114. Banerjee S, Kahn MG, Wong SS. 2003. Rational chemical strategies for carbon nanotube functionalization. *Chemistry* 9:1898–908
115. Bardin M, Loheac P, Petit M, Plichon V, Richard N. 1995. Electrochemical and mirage detection studies of sputtered iridium oxide. *New J. Chem.* 19:59–63
116. Troyk PR, Detlefsen DE, Cogan SF, Ehrlich J, Bak M, et al. 2004. "Safe" charge-injection waveforms for iridium oxide (AIROF) microelectrodes. *Proc. IEEE. Eng. Med. Biol. Soc.* 6:4141–44
117. Bard AJ, Faulkner LR. 2001. *Electrochemical Methods: Fundamentals and Applications*. New York: Wiley. 2nd ed.
118. Cogan SF, Troyk PR, Ehrlich J, Gasbarro CM, Plante TD. 2007. The influence of electrolyte composition on the in vitro charge-injection limits of activated iridium oxide (AIROF) stimulation electrodes. *J. Neural Eng.* 4:79–86
119. Suesserman MF, Spelman FA, Rubinstein JT. 1991. In vitro measurement and characterization of current density profiles produced by nonrecessed, simple recessed, and radially varying recessed stimulating electrodes. *IEEE Trans. Biomed. Eng.* 38:401–8
120. Cogan SF. 2006. In vitro and in vivo differences in the charge-injection and electrochemical properties of iridium oxide electrodes. *Proc. IEEE Eng. Med. Biol. Soc.* 8:886–89
121. Hu Z, Troyk PR, Brawn TP, Margoliash D, Cogan SF. 2006. In vitro and in vivo charge capacity of AIROF microelectrodes. *Conf. Proc. IEEE Eng. Med. Biol. Soc.* 1:886–89
122. Ballestrasse CL, Ruggeri RT, Beck TR. 1985. Calculations of the pH changes produced in body tissue by a spherical stimulation electrode. *Ann. Biomed. Eng.* 13:405–24

Annual Review of Biomedical Engineering
Volume 10, 2008

Contents

Indexes

Errata

An online log of corrections to *Annual Review of Biomedical Engineering* articles may be found at http://bioeng.annualreviews.org/